



CHAPTER 18

Cardiovascular Magnetic Resonance Imaging

Raymond Y. Kwong

BASIC PRINCIPLES OF MAGNETIC RESONANCE IMAGING, 340

Magnetic Field and Gradient Coil System, 340
Generation of Magnetic Resonance Signal, Signal Contrast, and Image Formation, 340
Contrast Agents, 341

TECHNICAL ASPECTS OF CARDIAC MAGNETIC RESONANCE PULSE SEQUENCES, 341

Contrast-Enhanced Imaging, 342

PATIENT SAFETY, 343

Performing Cardiac Magnetic Resonance in Patient with a Permanent Pacemaker or Defibrillator, 343

CLINICAL APPLICATIONS, 343

Assessment of Coronary Artery Disease, 343
Assessment of Cardiomyopathies, 346
Diastolic Dysfunction, 351
Pericardial Disease, 351
Adult Congenital Heart Disease, 352
Valvular Heart Disease, 354
Cardiac Thrombi and Masses, 354

NOVEL CARDIAC MAGNETIC RESONANCE IMAGING TECHNIQUES, 355

Magnetic Resonance Spectroscopy, 355
Cardiac Magnetic Resonance at 3 T, 356
Molecular Cardiac Magnetic Resonance Imaging, 357

FUTURE PERSPECTIVES, 357

REFERENCES, 357

APPROPRIATE USE CRITERIA, 359

Over the past decade, cardiac magnetic resonance (CMR) has developed into a routine clinical imaging tool. With excellent spatial and temporal resolution, unrestricted tomographic fields, and no exposure to ionizing radiation, CMR offers detailed morphologic and functional characterization for most types of heart disease. In this chapter, the current evidence supporting the use of CMR in the diagnosis and risk stratification of patients with heart disease will be reviewed and the future directions of this technology will be discussed.

Basic Principles of Magnetic Resonance Imaging

Magnetic Field and Gradient Coil System

Magnetic resonance imaging (MRI) is based on the imaging of water (and fat, to a lesser extent) because of its abundance in the body. The hydrogen nuclei (spins) within water or fat possess magnetic moment. When a patient is placed inside the CMR scanner within a static magnetic field (B_0), spins are either aligned with or opposite the main direction of B_0 . The summation of the net spins forms a magnetization vector that aligns along the longitudinal axis (z axis) of the magnet at static state before the deposition of any radiofrequency pulse (**Fig. 18-1**). The main B_0 field is created so that it has the same strength along each of the three orthogonal directions (known as x , y , and z) inside the CMR bore; thus, it is a homogeneous magnetic field. The homogeneous B_0 is fine-tuned by the computer-controlled adjustments of currents in small coils mounted within the magnet, a process known as active shimming. Apart from lining up with B_0 , spins also precess (wobble about the axis of the B_0 field) at a frequency ω_0 , known as the Larmor frequency, proportional to B_0 as described by the following equation:

$$\omega_0 = \gamma B_0$$

where γ is the gyromagnetic ratio (a constant for hydrogen for a given field strength). To introduce a system of spatial address of the Larmor frequency, three orthogonal sets of gradient coils are placed so that a slight linear alteration in the strength of B_0 can be created in each of the x , y , and z directions. As a result, magnetic spins precess at frequencies according to their locations along each of the three orthogonal axes and they can be excited selectively by specific radiofrequency pulses.

Generation of Magnetic Resonance Signal, Signal Contrast, and Image Formation

Magnetic resonance is a form of energy exchange between spins and a radiofrequency (RF) pulse that can only occur at a specific frequency. To create an image, an RF pulse with a frequency matched to the Larmor frequency of the magnetic spins will excite magnetic spins of interests to a higher energy state, which leads to a tipping down of the net magnetization vector from the z axis onto the x - y plane. There is, therefore, an increase of the transverse component (onto the x - y plane) and a decrease of the longitudinal component (z axis) of the net magnetization vector. The extent to which the magnetization vector is tipped away from the direction of B_0 (z axis) defines the flip angle, reflects the amount of energy deposition in tissue, and is a function of the strength and duration of the RF pulse. A set of phased array surface coils in front and behind the patient's chest is used to receive the magnetic resonance signal generated. For the purpose of imaging thin cross sections through the body, an RF pulse should only "excite" spins in that cross section and have no effect elsewhere. This can be achieved by applying a magnetic field gradient perpendicular to a prescribed slice plane; the magnetic gradient causes a spread of Larmor frequencies, and the resonance condition for the RF excitation is only met by a thin cross section whose width is determined by the frequency bandwidth of the RF pulse.

The absorbed electromagnetic energy by the spins will be released by two coexisting mechanisms termed *longitudinal magnetization recovery* and *transverse magnetization decay*. Longitudinal magnetization recovery corresponds to the exponential rate of recovery of the longitudinal component (z direction) of the net magnetization vector, characterized by the time constant T_1 , which is defined as the time to recover 63% of the original longitudinal magnetization vector. T_1 is a physical characteristic of the tissue of interest, but is also affected by the field strength of the scanner, with values progressively longer at higher field strengths (in Tesla). The variation of T_1 between tissue types allows one to generate images that reflect these differences. A T_1 -weighted scan will keep the time between delivery of two successive flip angles (repetition time) short, thus maximizing the sensitivity to differentiating tissues by the displayed signal intensity as a result of difference in their T_1 values. The transverse magnetization decay results from interaction between neighboring spins (spin-spin interaction) leading to exponential loss of the transverse component of the net magnetization vector, defined by the time constant T_2 . T_2 is also a tissue-specific parameter and is defined as the time to lose 63% of

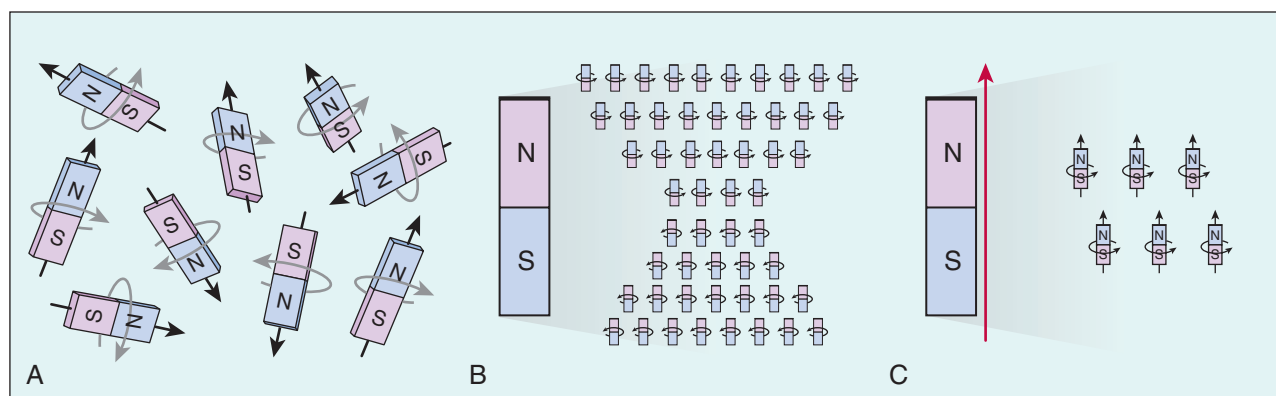


FIGURE 18-1 **A**, Spins are randomly oriented in the absence of an external magnetic field. **B**, In the presence of an external magnetic field, B_0 , the spins align parallel or antiparallel to it. **C**, The difference between the parallel minus the antiparallel spins represents the spins that will create a detectable magnetic resonance signal. (Modified from Aletras AH: *Basic MRI physics*. In Kwong RY (ed): *Cardiovascular Magnetic Resonance Imaging*. Totowa, NJ, Humana Press, 2008, pp 1-32.)

the transverse magnetization. Unlike T1, T2 values are unrelated to the field strength of the scanner. To distinguish different tissues, contrast must be obtained, which is the difference in the magnetic resonance signals of two structures of interest. These depend on the T1, T2, and proton density of the tissues and sequence parameters. With the application of magnetic field gradients in any of the three orthogonal directions, the magnetic resonance signal can carry spatial localization information, produced by encoding steps known as slice select, phase encoding, and frequency encoding. All relevant information of the magnetic resonance signal is stored in a data matrix called the k-space, which will undergo two-dimensional inverse Fourier transformation to form an image. The choice of signal contrast weighting of the imaging method is partly dictated by the physiologic characteristics of the tissue being studied. For qualitative interpretation, signal enhancement (from T1 effects) is in general preferred over darkening (T2*) effects (see later); thus, most pulse sequences used in CMR are relative T1-weighted signal-enhancing techniques. In addition, T1-weighted pulse sequences are less prone to artifacts from adjacent air in the lungs or from cardiac motion.

Contrast Agents

For practical purposes, gadolinium-based contrast agents (GBCAs) are the only contrast materials used in clinical MRI today. After intravenous injection, a GBCA typically takes 15 to 30 seconds for a first pass through the cardiac chambers and blood vessels (first-pass phase) before it diffuses into the extracellular space. At approximately 10 to 15 minutes after injection, a transient plateau of GBCA concentration (equilibrium between contrast washing in to the extracellular space and washing out to the blood pool) is reached. Myocardial perfusion CMR and most types of magnetic resonance angiography (MRA) are performed during the first-pass phase, whereas late gadolinium enhancement (LGE) images are obtained during the equilibrium phase. There are several commercially available GBCAs in the United States, but their use in CMR is considered off-label. Mild allergic reactions from GBCA occur in 0.01% to 0.07% of patients but severe or anaphylactic reactions are rare. All GBCAs are chelated to make the compounds nontoxic and to allow renal excretion. Exposure to the nonchelated component of GBCA (Gd^{3+}) has been reported to trigger nephrogenic systemic fibrosis (NSF), which is characterized by an interstitial inflammatory reaction that leads to severe skin induration, contracture of the extremities, fibrosis of internal organs, and even death. Risk factors for developing NSF include a high-dose (>0.1 mmol/kg) of GBCA in the setting of renal insufficiency (estimated glomerular filtration rate [eGFR] < 30 mL/min/1.73 m²), need for hemodialysis, severe renal insufficiency (eGFR < 15 mL/min/1.73 m²), acute renal failure, presence of concurrent proinflammatory processes, and use of the specific GBCA gadodiamide (Omniscan, General Electric Healthcare). A recent review from high-volume MRI centers has shown that NSF is rare. Wertman and colleagues¹ have reviewed

records over 7 years at four major U.S. tertiary care centers and reported an NSF incidence of 0.002% to 0.3%, depending on the agent used. Prince and associates² have reported an overall incidence of 0.02% in 83,121 patients exposed to GBCA over 10 years when routine screening for renal function was not performed. Most MRI facilities have been screening for high-risk patients in the past few years, and the reported incidence of NSF has been near zero.

TECHNICAL ASPECTS OF CARDIAC MAGNETIC RESONANCE PULSE SEQUENCES

CMR uses a range of strategies to overcome technical difficulties caused by cardiac motion, respiratory motion, and blood flow. Collection of data synchronized to the cardiac cycle (gating) is required, and thus careful placement of electrodes to obtain a reliable electrocardiographic signal is crucial. Fortunately, advances in gating technology have allowed reliable cardiac gating in almost all patients in 1.5-T and even 3-T scanners. Cardiac gating can be prospective (triggering by an electrocardiographic waveform followed by a fixed period of acquisition during all cardiac cycles) or retrospective (continuous data acquisition with subsequent reconstruction based on electrocardiographic timing). For cine imaging, retrospective gating is preferred because it covers the entire cardiac cycle and does not have the flash artifact—sudden brightness of images in the cine loop from partial recovery of longitudinal magnetization—seen in prospective gating. To reduce blurring from cardiac motion, many CMR techniques fractionate the data for an image to be acquired only within a narrow window of the cardiac cycle (segmented approach). On the other hand, other techniques can rapidly acquire data of an entire image all within a cardiac cycle (single-shot approach), thus eliminating the need for breath-holding but at the expense of lower spatial resolution and increased blurriness. Respiratory motion is contained in most situations currently by using a 5- to 15-second breath-hold if compatible with the patient's clinical conditions. Otherwise, navigator-based techniques (tracking of diaphragmatic motion to achieve combined electrocardiographic and diaphragmatic motion gating) and respiratory motion averaging are alternative strategies to suppress respiratory motion. Finally, real-time imaging involves rapid and continuous acquisition of single-shot images that overcomes respiratory and cardiac motion, but at the expense of reduced temporal and spatial resolutions.

Table 18-e1 (see website) provides a summary of the most common clinical CMR pulse sequence techniques at our center. Variations in these parameters exist among centers. CMR uses bright blood cine imaging or dark blood fast spin-echo (FSE) imaging to assess cardiac morphology and structure. Cine CMR has become the imaging reference standard for quantifying ventricular volumes, mass, and regional and global contractile function because of its lack of need for geometric assumption. Among the various cine CMR techniques, cine steady state with free precession (SSFP) is the current technique of choice for its highest image quality. It can acquire a cine movie at a high temporal resolution of 30 to 45 milliseconds during a breath-hold of less than 10 seconds, so that the whole heart in motion is captured in less than 5 minutes. T1-weighted dark blood FSE has high spatial resolution and is often used for the morphology of cardiac chambers, vascular structures, pericardium, and imaging of fat. CMR techniques have been developed to quantify intramyocardial motion to overcome the interobserver variation of visualizing

regional wall motion. There are three main methods used—myocardial grid or line tagging, phase contrast velocity mapping of myocardial motion, and displacement encoding with stimulated echoes (DENSE). Tagging assesses myocardial strain by marking the myocardium with a geometric pattern (dark lines or grid) using selective spatial presaturation pulses or spatial modulation of magnetization (SPAMM), so that myocardial deformation can be visualized or quantified. Circumferential and radial strains (often abbreviated as E_{cc} and E_{rr} , respectively) can also be calculated and displayed with a color-coded scale. Although myocardial tagging is the most widely available, phase contrast velocity mapping and DENSE techniques can perform at higher spatial resolutions. With similarities to Doppler echocardiography (see Chap. 15), phase contrast imaging allows quantitation of velocities of blood flow and myocardial motion and intravascular flow rates.

Contrast-Enhanced Imaging

When the extracellular compartment of the myocardium is enlarged because of infarction, infiltration, or replacement fibrosis, influx and retention of the GBCA can be seen by T1-weighted imaging such as LGE. LGE is best detected 10 to 15 minutes after an intravenous injection of GBCA (0.1 to 0.2 mmol/kg)—hence the term *late gadolinium enhancement*. **Figure 18-2** illustrates this technique with LGE imaging of a patient with an anterior myocardial infarction (MI). Further details regarding the features of this pulse sequence are shown in Table 18-e1 (see website). Currently, both two-dimensional and three-dimensional techniques are available; each has its respective merits. A recent technique termed *phase-sensitive inversion recovery* (PSIR) reference imaging incorporates

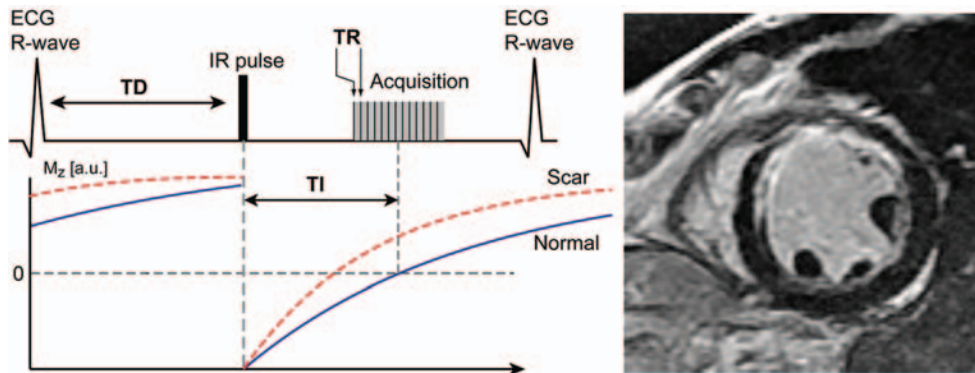


FIGURE 18-2 T1-weighted inversion recovery fast gradient echo imaging for LGE. The technique uses the difference in T1 between infarcted (T1 shortened by accumulation of gadolinium) and normal myocardium. Imaging data acquisition is set to occur at the appropriate inversion time when normal myocardium is nulled (dark) and during mid-late diastole to minimize motion blurring. The image shows differentiation of a bright infarcted anterior wall, intermediate-intensity blood pool, and dark normal myocardium.

the phase polarity information, which further enhances myocardial tissue contrast.³ In addition, single-shot approaches or the use of navigator guidance are increasingly used in clinical studies to eliminate the need for breath-holding.^{4,5}

CMR perfusion imaging examines the first-pass transit of an intravenous bolus of GBCA as it travels through the coronary circulation. A comprehensive review of the CMR perfusion pulse sequence design and applications can be found elsewhere.⁶ In myocardial perfusion studies, ultrafast pulse sequence techniques are used to acquire three to five short-axis slices of the heart at every heartbeat during injection of a bolus of GBCA. Gadolinium provides strong signal enhancement in well-perfused regions compared with poorly perfused myocardium, which appears to be hypoenhanced (darkened). At a spatial resolution of approximately 2 mm in-plane, CMR perfusion imaging can provide information regarding myocardial blood flow at the endocardial-epicardial level or at the level of the American College of Cardiology/American Heart Association (ACC/AHA) 17-segment model. Newer methods, such as SSFP and 3-T perfusion imaging, which provide a substantially higher signal-to-noise-ratio, are promising to improve image quality further.⁷ T2-weighted imaging detects myocardial edema as a result of ischemic injury or inflammation. The edematous region obtained by T2-weighted imaging has been shown to have high correlation to the area at risk after an acute MI (see Fig. 58-4).⁸ T2-weighted imaging complements LGE in determining the chronicity of MI and allowing for sizing of salvageable myocardium after emergent revascularization. The pulse sequence options, including the widely used black blood short inversion time inversion

recovery (STIR) FSE and newer SSFP methods, and their merits are listed in Table 18-e1 (see website).^{9,10}

T2* is a transverse relaxation parameter sensitive to tissue iron content. T2* imaging has been extensively validated at 1.5 T against tissue iron levels with excellent interstudy reproducibility over time and across different MRI platforms.^{11,12} A T2* shorter than 20 milliseconds (normal myocardium, ~40 to 50 milliseconds) is diagnostic of myocardial iron overload and a T2* shorter than 10 milliseconds is evidence of severe iron overload.^{13,14} Despite challenges from small luminal sizes, vessel tortuosity, and cardiac and respiratory motions, technical advances in coronary MRA imaging have resulted in high success rates in experienced centers¹⁵⁻¹⁷ (**Fig. 18-3**). Currently, the common technique acquires a three-dimensional heart volume using navigator guidance

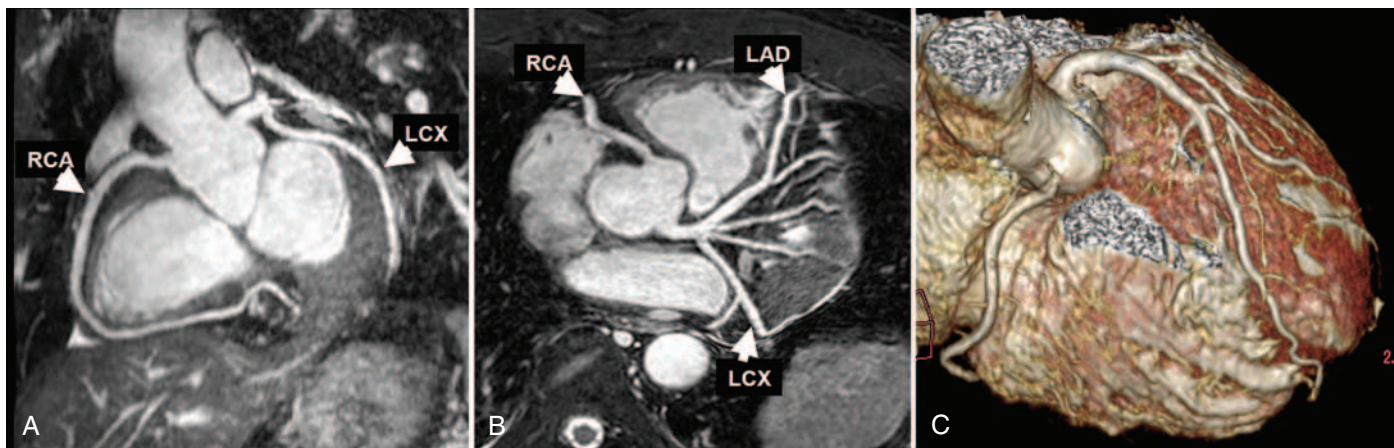


FIGURE 18-3 Free-breathing, navigator echo-gated whole-heart coronary MRA acquired with an SSFP sequence (balanced turbo field echo) with fat saturation and T2 preparation in a subject with normal coronary arteries. **A**, Left anterior oblique whole-heart coronary MRA reformatted with curved multiplanar reformatting clearly depicts the right coronary artery (RCA) and left circumflex (LCX) arteries. **B**, Oblique axial whole-heart coronary MRA reformatted with curved multiplanar reformatting visualizes the left main coronary artery, left anterior descending (LAD) artery, proximal RCA, and LCX artery. **C**, Volume-rendered image of whole-heart coronary MRA is useful for three-dimensional anatomic recognition of the coronary arteries. (From Sakuma H, Ichikawa Y, Suzawa N, et al: Assessment of coronary arteries with total study time of less than 30 minutes by using whole-heart coronary MR angiography. *Radiology* 237:316, 2005.)

at a spatial resolution (0.8×0.8 mm at a slice thickness of 1 mm) that is only slightly lower than computed tomography (CT; see Chap. 19). A recent consensus statement from the AHA has assigned a level of evidence of IIa for evidence supporting the use of coronary MRA in assessing coronary anomalies.¹⁵

Many parallel imaging techniques are routinely used to speed up CMR (k-space) data acquisition while cardiac and respiratory motions are controlled for image quality. These techniques combine information obtained separately from each element of the surface receiver coil to reduce the sampling of k-space data for faster image acquisition. Incorporating parallel imaging into pulse sequences can lead to reduced acquisition time, shorter patient breath-holds, improved temporal resolution, and/or elimination of certain artifacts. The main disadvantage of all parallel imaging techniques is a reduction in signal-to-noise ratio as a result of undersampling of the k-space lines.

Patient Safety

Most clinical (1.5-T) CMR scanners are superconducting systems in which the magnetic field created by the superconductive coil cannot be turned off. In rare emergency situations, the only way to remove the magnetic field quickly is by rapidly boiling off the cooling liquid helium as gas to the outside environment (quenching) through evacuation pipes. Every caution must be practiced to avoid an emergency quench because it carries the risk of burns or asphyxia to individuals inside the MRI scanner room, and restoration of the magnetic field is costly. A short list of common medical devices that are contraindications to the use of CMR include cochlear implants, neurostimulators, hydrocephalus shunts, metal-containing ocular implants, pacing wires, Swan-Ganz catheters, and metallic cerebral aneurysm clips. Sternal wires, mechanical heart valves and annuloplasty rings, coronary stents, nonmetallic catheters, and orthopedic or dental implants can be safely scanned at 1.5 T and even 3 T (updated safety information for medical devices can be found at www.mrisafety.com). Patient claustrophobia can almost always be managed with oral sedation or by performing the study in a short-bore scanner with an expanded diameter.

Performing Cardiac Magnetic Resonance in Patient with a Permanent Pacemaker or Defibrillator

The risks of performing MRI in the presence of a pacemaker or automated implantable cardioverter-defibrillator (ICD) include the generation of an electrical current from the metallic hardware (especially if wire loops exist), device movement induced by the magnetic field, inappropriate discharging and sensing, and heating as a result of the antenna effect.¹⁸ A temporary pacemaker is currently an absolute contraindication to CMR, although clinical trials of pacemakers with new designs of pacing wires are underway. A number of experienced centers have reported safety in performing CMR at 1.5 T in patients with a permanent pacemaker. Roguin and coworkers¹⁹ have reported safe and successful MRI examinations in 99% of patients using an algorithm involving careful selection and programming of the pacemaker and limiting the RF energy absorbed by the patient to less than 2.0 W/kg by any pulse sequence. A similar strategy was reported to be safe by the same group, which allowed non-pacemaker-dependent patients with ICDs implanted after 2000 to undergo CMR.²⁰ Collectively, evidence from combined reports of more than 250 patients in the medical literature with pacemaker models from the year 2000 or later appears to suggest that CMR at 1.5 T or less can be safely performed in a controlled setting.

Clinical Applications

The next sections of this chapter discuss clinical aspects of CMR imaging. Table 18-e2 (see website) provides a summary of the CMR protocols by study indications at our center. A detailed description of CMR protocols endorsed by the Society of Cardiovascular Magnetic Resonance (SCMR) is available at www.scmr.org.²¹ In addition, the

SCMR has established reporting guidelines to provide a framework for enhancing communication with referring physicians.²²

Assessment of Coronary Artery Disease

Multicomponent CMR imaging is capable of characterizing various pathophysiologic states described within the spectrum of coronary artery disease (CAD). Current CMR protocols for CAD integrate cine SSFP, T2-weighted edema imaging, myocardial perfusion at rest and stress, and LGE imaging of myocardial scar, thus providing a comprehensive evaluation of myocardial anatomy and physiology. Coronary MRA is also performed as a part of the CMR examination in more experienced centers. Tables 18-e2 and 18-e3 (see website) summarize the CMR protocols used in our center and the typical CMR findings of CAD.

IMAGING OF MYOCARDIAL INFARCTION. LGE imaging is currently the most accurate and precise noninvasive method to quantify infarct size and morphology in patients (see Figs. 58-14 and 56-5).²³ There are easy-to-use commercial software programs and more sophisticated validated computer algorithms available for in vivo quantitation of infarct size by LGE.²⁴ At the clinical level, infarct size or infarct transmural by LGE imaging correlates with markers of infarct size such as serum creatine kinase level, time to treatment, and incomplete electrocardiographic ST-segment resolution.¹⁷ The robustness of the LGE imaging across MRI vendors was demonstrated by a recent double-blind, multicenter, randomized trial of 566 patients who underwent LGE imaging for MI.²⁵ LGE identified infarct location accurately and detected acute and chronic infarcts with a sensitivity of 99% and 94%, respectively. When LGE imaging is performed early (within the first 5 minutes) after contrast injection, regions of microvascular obstruction (no-reflow) can be seen as a dense hypoenhanced area within the core of a bright region of infarction (Fig. 18-4). This noninvasive method for quantifying microvascular obstruction has been validated against angiographic parameters of microcirculatory flow such as thrombolysis in myocardial infarction (TIMI) frame counts, intracoronary Doppler flow, and myocardial blush score.¹⁹ A recent study has demonstrated detection of myocardial hemorrhage as a result of reperfusion injury.²⁶

With an in-plane spatial resolution of 1.5 to 2 mm and a high contrast-to-noise ratio, LGE imaging can recognize subendocardial MI undetected by single-photon emission computed tomography (SPECT) or positron emission tomography (PET). This high sensitivity of LGE in detecting MI has been shown to detect down to a few grams of infarcted tissue in the target myocardial region of distal embolization during percutaneous coronary intervention in patients with CAD.²⁷ There is growing evidence that these technical advantages of CMR translate to useful patient prognostic information. In a study of 195 patients referred for assessment of CAD but without a history of MI, LGE consistent with an unrecognized MI was an independent and strong predictor of cardiac death after adjustment to common clinical variables. Even infarct size in the smallest tertile was associated with a more than sevenfold unadjusted hazard of adverse events.²⁸

Patients with diabetes are a particular subgroup with a high likelihood of unrecognized previous coronary events (see Chap. 64). In a study of 187 diabetics undergoing CMR for assessment of CAD, patients without clinical or electrocardiographic evidence of MI experienced a 3.6-fold elevated hazard of death if LGE consistent with MI was detected, with a Kaplan-Meier distribution for cardiac death similar to that of diabetic patients known to have had a clinical MI²⁹ (Fig. 18-5).

Other studies support the prognostic value of LGE in patients with clinically recognized MI. A recent study of 857 patients by Cheong and colleagues³⁰ has reported that LGE scar transmural index is a strong independent predictor of death or cardiac transplantation at a median follow-up of 4.4 years; this provides complementary prognostic information to the left ventricular (LV) ejection fraction (Fig. 18-6). The same investigators also reported that LGE provides similar prognostic information in a subgroup of 349 patients with CAD and severe LV dysfunction.³¹ Several pilot studies have demonstrated that tissue inhomogeneity quantified in LGE images may identify arrhythmogenic



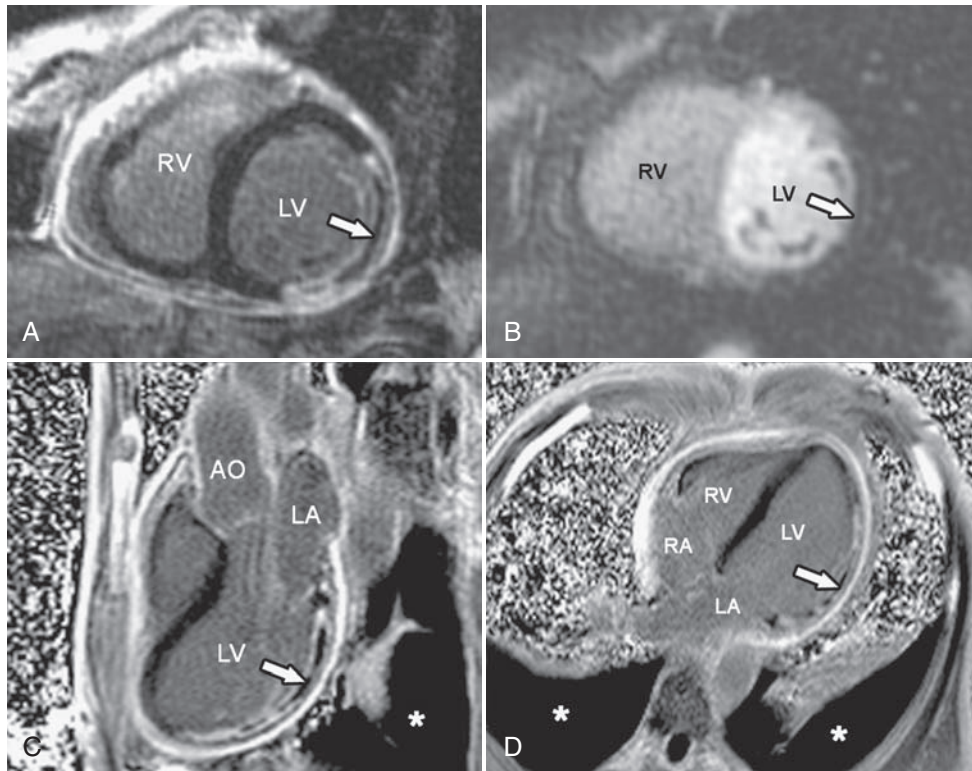


FIGURE 18-4 A 52-year-old man with history of a prior inferior MI 1 week ago was referred for assessment of myocardial viability. **A**, Short-axis LGE images reveal a transmural MI involving the lateral LV wall associated with a large and dense area of microvascular obstruction (arrow). **B**, Despite successful epicardial revascularization of the infarct-related coronary artery, first-pass myocardial perfusion imaging demonstrates a dense perfusion defect indicative of no-reflow (arrow) matching in location with the infarct. **C, D**, Long-axis LGE images confirm the extensive area of microvascular obstruction involving a large extent of the lateral LV wall. Of note, there was concurrent intense pericardial inflammation and bilateral pleural effusion (asterisk). Ao = aorta; LA = left atrium; RA = right atrium; RV = right ventricle.

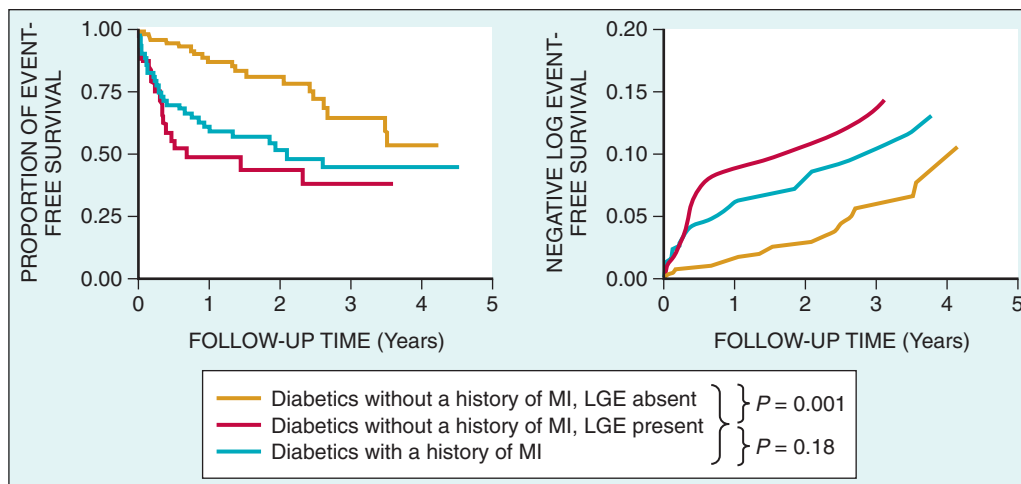


FIGURE 18-5 Kaplan-Meier event-free survival curves (**left panel**) and cumulative rate of adverse cardiac events (**right panel**) for patients with diabetes. Patients without a history of MI who had no evidence of infarction by LGE imaging (yellow curve) experienced a relatively benign clinical course, compared with worse event-free survival in patients with a known history of MI (blue curve) and patients without a history of MI who had evidence of unrecognized MI by LGE imaging (red curve). (From Kwong RY, Sattar H, Wu H, et al: Incidence and prognostic implication of unrecognized myocardial scar characterized by cardiac magnetic resonance in diabetic patients without clinical evidence of myocardial infarction. *Circulation* 118:1011, 2008.)

substrates that develop as a result of MI. Schmidt and associates³² have reported a method for quantifying the heterogeneous peri-infarct zone, which demonstrated a strong association with inducible monomorphic ventricular tachycardia during electrophysiologic studies. Roes and coworkers,³³ using slightly different quantitative criteria, have reported that the peri-infarct zone is the strongest predictor of spontaneous ventricular arrhythmias that required appropriate ICD therapy in 91 patients with previous MI in whom ICDs were implanted

for clinical indications. These findings are concordant with the observed increased in patient mortality associated with larger peri-infarct zones in a cohort of 144 post-MI patients reported by Yan and colleagues³⁴ (**Fig. 18-7**). Before this promising novel application can become a routine means of stratifying patients according to arrhythmic risks, future studies need to establish standardized criteria for quantifying the peri-infarct zone and demonstrate robustness in its association with serious arrhythmic events.

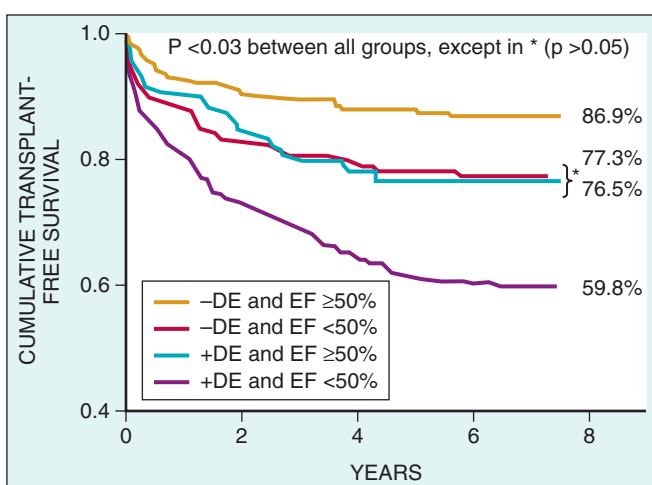


FIGURE 18-6 Transplant-free survival in a cohort of 857 patients referred for CMR assessment of coronary artery disease. Patients are stratified by left ventricular ejection fraction (EF) and the presence (+) or absence (–) of delayed contrast enhancement (DE). (From Cheong BYC, Muthupillai R, Wilson JM, et al: Prognostic significance of delayed-enhancement magnetic resonance imaging. *Circulation* 120:2069, 2009.)

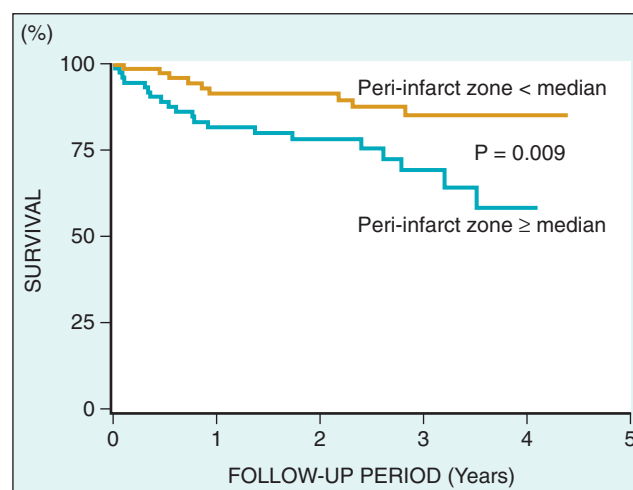


FIGURE 18-7 Kaplan-Meier survival curves for all-cause mortality, stratified by median size of the peri-infarct zone. (From Yan AT, Shayne AJ, Brown KA, et al: Characterization of the peri-infarct zone by contrast-enhanced cardiac magnetic resonance imaging is a powerful predictor of post-myocardial infarction mortality. *Circulation* 114:32, 2006.)

ASSESSMENT OF MYOCARDIAL VIABILITY AND BENEFIT FROM CORONARY REVASCUARIZATION. Several pitfalls are often encountered in the imaging of myocardial viability. A fundamental concept defines myocardial viability as preservation of cellular function without any irreversible cellular damage. Although assessment of histologic viability could not be reliably achieved clinically, indirect markers of cellular function have been used as surrogates of myocardial viability and have created problems in comparing the usefulness of various noninvasive modalities. Recovery of regional and/or global LV systolic function after coronary revascularization is the most common clinical standard of myocardial viability, but this surrogate provides limited information about patient morbidity and mortality. Targeting different cellular processes of the hibernating myocardium, imaging modalities can yield discordant results at different stages or severity of chronic hypoperfusion, causing inconsistencies when the usefulness of these imaging modalities are compared. Consider the following two examples: (1) early development of ischemia in myocardium subtended by a critical coronary stenosis during low-dose dobutamine challenge (see Chap. 15); and (2) lack of contractile reserve when chronic and severe hypoperfusion has led to disassembly of cellular contractile filaments and myocyte dedifferentiation (see Chap. 52), despite maintenance of basic cellular metabolism and cell membrane integrity. In both these examples, the absence of contractile reserve would suggest a lack of viability. Other techniques, such as PET, which detects myocardial metabolism (see Chap. 17), or LGE imaging by CMR, which detects altered tissue relaxation characteristics of irreversibly injured myocardium, may identify these segments as viable in either example. However, recovery of contractile function, which may occur in the first example, is unlikely in the second.

End-diastolic wall thickness alone has limited accuracy in predicting the recovery of segmental function because it may include irreversibly damaged subendocardial myocardium and a thinned epicardial rim of viable myocardium, which may not be sufficient to result in improved function after successful coronary revascularization. In addition, during acute ischemia, local edema and cellular infiltrates may increase regional wall thickness. Augmentation of regional function in response to low-dose (5 to 10 $\mu\text{g}/\text{kg}/\text{min}$) dobutamine administration has been well validated in identifying segmental viability by cine CMR. Early cine CMR studies showed that contractile reserve, defined as an increase in systolic wall thickening of 2 mm, has excellent specificity and sensitivity in predicting segmental contractile recovery after revascularization (sensitivity, 89%; specificity, 94%).

In a landmark paper by Kim and associates,³⁵ the transmural extent of myocardial scar detected by LGE imaging was shown to predict a progressive stepwise decrease in the likelihood of function recovery accurately, despite successful coronary revascularization. This prediction of segmental functional recovery was especially strong in segments with resting akinesia or dyskinesia. For example, 88% of segments with less than 25% transmural extent of LGE improved contractile function, whereas only 4% of segments with more than 50% transmural extent of

LGE improved function after revascularization. Compared with dobutamine cine CMR, LGE is easy to perform and interpret, and a 50% transmural cutoff is sensitive in predicting segmental contractile recovery. On the other hand, the high specificity of low-dose dobutamine cine CMR provides a physiologic assessment of the midmyocardial and subepicardial contractile reserve, particularly in segments with subendocardial infarction involving less than 50% of the transmural extent. Some controversy exists as to whether dobutamine cine CMR provides additional information beyond LGE characterization of infarct transmural extent in this setting. Among a few other single-center studies, Wellnhofer and coworkers³⁶ assessed 29 patients before and 3 months after coronary revascularization with both low-dose dobutamine cine imaging and LGE imaging, and reported better prediction of segmental contractile recovery by dobutamine cine imaging. Although local expertise and difference in opinion will continue to direct regional practice, at our center it appears that LGE imaging alone suffices to answer most questions about assessing myocardial viability. However, low-dose dobutamine cine CMR can be complementary in assessing myocardial viability early after acute MI when tissue edema is prominent or when there is a need to assess the benefit of bypass surgery in patients at high preoperative risk.

DETECTING ACUTE CORONARY SYNDROMES AND DIFFERENTIATING FROM NONCORONARY CAUSES. Early studies performed in the emergency department setting indicated high sensitivity and specificity of CMR in detecting acute coronary syndromes and in risk-stratifying patients presenting with acute chest pain.^{37,38} Abdel-Aty and colleagues³⁹ have studied 73 post-MI patients and found that qualitative assessment of T2-weighted imaging and LGE yielded a 96% specificity in differentiating acute from chronic MI. Cury and associates⁴⁰ have assessed patients presenting with acute chest pain with negative electrocardiographic findings and cardiac enzyme levels. They reported that adding T2-weighted imaging and LV wall thickness to cine and LGE imaging increases the specificity from 84% to 96% without any loss of sensitivity, thus enhancing the diagnostic certainty for acute coronary syndrome, especially in patients with prior MI. Furthermore, in patients presenting with acute chest pain, several single-center studies have reported strong diagnostic usefulness of CMR in differentiating acute coronary syndrome from non-coronary causes of chest pain.⁴¹⁻⁴³

DETECTING AND QUANTIFYING MYOCARDIAL ISCHEMIA

Myocardial Perfusion Imaging

Numerous single-center studies and a recent multicenter study have shown that qualitative assessment of vasodilator stress CMR myocardial perfusion is rapid and accurate in detecting CAD. Improved standardization of perfusion data acquisition and analysis across CMR centers and scanner manufacturers have been developed in the past few years. Klem and coworkers⁴⁴ have proposed and validated a





practical algorithm for the rapid diagnosis of CAD that combines information from stress and rest perfusion and LGE imaging. Plein and colleagues⁴⁵ demonstrated that combined interpretation of perfusion, coronary MRA, LGE, and cine CMR reaches an excellent sensitivity of 96% while maintaining a high specificity of 83% in detecting coronary stenosis in a prospective study of patients presenting with acute chest pain. The combined multicomponent CMR approach provides higher accuracy than any single CMR component alone.

There are several technical advantages of CMR stress perfusion over radionuclide perfusion imaging. CMR perfusion imaging is not limited by attenuation artifacts, has no need for ionizing radiation, and has three- to fourfold higher spatial resolution than SPECT. A stress CMR study that includes stress and rest perfusion imaging, cine cardiac function, and viability takes 35 to 45 minutes (compared with >2 hours for SPECT). CMR perfusion also can characterize the dynamic range of myocardial blood flow without being limited by the plateau effect of counts at high flow rates, as seen with almost all nuclear tracers (see Chap. 17).⁴⁶ In a recent multicenter trial (MR-IMPACT) conducted in 18 experienced centers that enrolled 241 patients who underwent coronary angiography,^{46a} CMR perfusion performed better than SPECT in detecting coronary stenosis (area under the curve, 86% versus 67%; $P = 0.01$), especially in the group of patients with multivessel stenosis (area under curve by CMR, 89% versus 70%, $P = 0.006$). This supports the notion that the higher spatial resolution obtained when characterizing subendocardial perfusion deficits by CMR may improve the detection of diffuse coronary disease as suggested by preclinical studies. CMR myocardial perfusion can also be analyzed by quantitative methods using the signal intensity versus time curves derived from LV myocardial segments. Accounting for arterial input function at different hemodynamic states and using a low dose of contrast injection—to maintain a linear relationship between contrast concentration and measured signal intensity—are prerequisites in quantitative methods. Common semiquantitative parameters include signal upslope (rate of rise of the ascending curve), upslope integral (area under the upslope), and contrast enhancement ratio (ratio of peak to baseline signal intensity; Fig. 18-8). Fully quantitative analysis of CMR perfusion yields absolute myocardial blood flow (in milliliters per minute per gram of tissue) using deconvolution methods and modeled compartmental analysis. The advantages of quantitative analyses include minimization of reader's bias and generation of color-coded maps of perfusion reserve (ratio of stress over rest myocardial blood flow), which may serve not only to improve the diagnosis of CAD but may test the efficacy of novel therapies.

Dobutamine Stress Cardiac Magnetic Resonance

Dobutamine stress CMR has been shown in several studies to have high sensitivities of 83% to 86% and specificities of 83% to 86% in detecting CAD and to be superior to dobutamine stress echocardiography when echocardiographic windows are inadequate, despite the use of second harmonic imaging. Such favorable results were consistent and maintained despite the presence of underlying resting wall motion abnormalities.⁴⁷ The addition of dobutamine stress myocardial perfusion imaging and myocardial tagging can serve as adjuncts to cine CMR for detecting myocardial ischemia.⁴⁸ Preliminary results of accelerated real-time cine CMR imaging, which eliminates the need for breath-holding or ECG gating during dobutamine stress, have been encouraging. Treadmill exercise CMR is currently investigational but has been shown to be feasible in highly experienced centers.

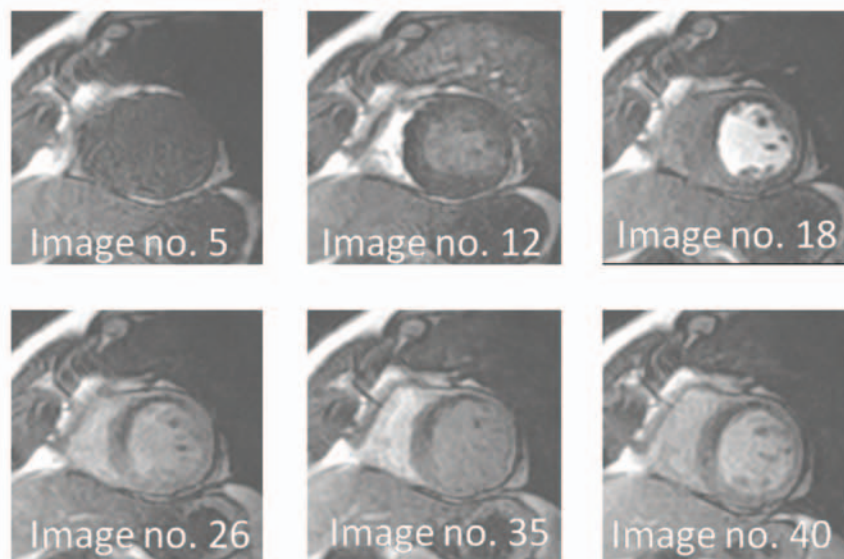
PROGNOSTIC VALUE. A growing number of studies have demonstrated strong prognostic values of stress CMR. Ingkanisorn and associates³⁷ have used adenosine stress CMR perfusion to assess 135 patients evaluated in the emergency department setting with chest pain but without electrocardiographic or serologic evidence of MI. At study follow-up, 20 patients developed clinical events (new diagnosis of significant coronary stenosis or adverse cardiac events). Stress CMR perfusion imaging was the strongest component of the CMR examination, with a sensitivity of 100% and specificity of 93% for clinical events at 1 year. Combining data from the components of a CMR study appears to provide complementary prognostic information. In a study of 513 patients, Jahnke and coworkers⁴⁹ have reported that a CMR study with normal dobutamine stress cine and normal adenosine perfusion carries a 99.2% negative 3-year event

rate for cardiac death or acute MI. In another study of 254 patients referred for stress CMR, Steel and colleagues⁵⁰ found robust and complementary prognostic information of stress CMR perfusion and LGE imaging in predicting cardiac death or acute MI. In that study, the presence of LGE, despite the absence of ischemia by stress or rest perfusion, was associated with an 11-fold increase in the hazard of cardiac death or acute MI. In a pilot study of 81 patients with angiographic stenosis of intermediate severity (50% to 75%) treated with medical therapy and followed for an average of 30 months, CMR perfusion was abnormal in all 9 patients who developed adverse events.⁵¹ Dobutamine stress CMR provides accurate patient prognostication beyond traditional coronary risk factors in patients referred for stress testing for evaluation of new symptoms or risk assessment before noncardiac surgery. In patients with normal dobutamine stress CMR, the cardiac event rate is less than 1% over the next 2 to 3 years in the presence of normal resting LV ejection fraction⁴⁹ and is only 2% in the presence of pre-existing global LV dysfunction. In a study of 200 patients with global LV dysfunction, Dall'Armellina and associates⁵² have demonstrated that the dobutamine stress wall motion score index provides useful patient prognostication, especially in the group with a resting LV ejection fraction between 40% and 55%, with a more than threefold elevated hazard of experiencing hard cardiac events in those with abnormal dobutamine responses. The same investigators also reported that dobutamine stress CMR provides prognostic information regarding cardiac death or MI in women.⁵³

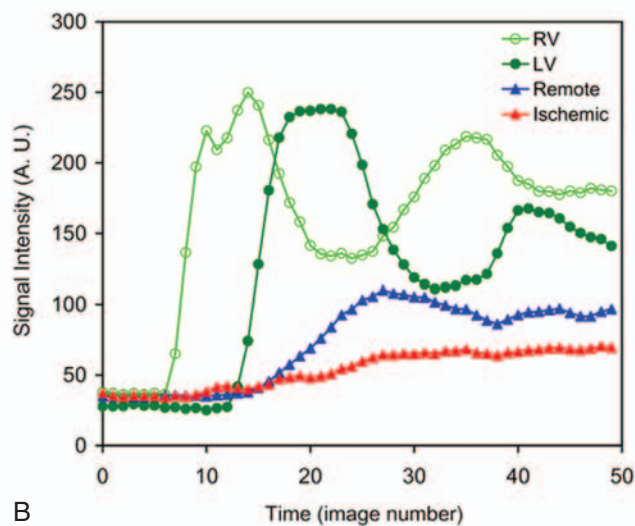
IMAGING OF ATHEROSCLEROTIC PLAQUES. Plaque structure and activity are important factors that lead to plaque vulnerability. MRI of the carotid artery and descending aorta remains the most comprehensive noninvasive method to characterize plaque structure and activity. The carotid bifurcation is relatively immobile, large, and superficial to the skin surface, and it shows the full spectrum of atherosclerotic lesion types. Yuan and Kerwin⁵⁴ have proposed a standardized protocol that consists of two contrast-weighted imaging sequences to identify carotid plaque fibrous cap, hemorrhage, calcifications, and loose matrix. In addition, gadolinium-enhanced T1-weighted imaging helps discriminate fibrous cap from necrotic or lipid core. Carotid plaque activity such as neovascularization can be assessed by contrast-enhanced dynamic MRI that measures the transfer constant between blood and the extracellular space, with preliminary evidence of prognostic implications.^{55,56} Ultrasmall superparamagnetic particles of iron oxide (USPIO) have been shown to target macrophage activity at high affinity based on histologic and electron microscopic analyses of atherosclerotic plaques. By causing signal darkening from the T2* susceptibility effect, USPIO-based CMR imaging of macrophages in carotid plaques can be performed with an optimal time window at 24 to 36 hours after USPIO injection.⁵⁷ MRI of aortic plaques is limited by signal-noise ratio in achieving submillimeter spatial resolution and blood flow artifacts. Technical improvements in aortic plaque imaging using intravascular magnetic resonance coils have been reported.⁵⁸ CMR provides accurate quantitation of aortic plaque size and composition, which complements three-dimensional MRA assessment of the thoracic aorta. Common to all imaging modalities, imaging of the coronary plaque is challenged by cardiac and respiratory motion and small vessel size, but future technical improvement using exogenous targeted contrast agents, intravascular coils, and high-field CMR may offer promise. Specifically, the fibrin-binding contrast agent EP-2104R (EPIX Pharmaceuticals, Cambridge, Mass) has been shown to allow CMR imaging of coronary thrombosis.⁵⁹ This molecule-targeting approach is advantageous because the demands for high spatial resolution and motion suppression may be less stringent.

Assessment of Cardiomyopathies

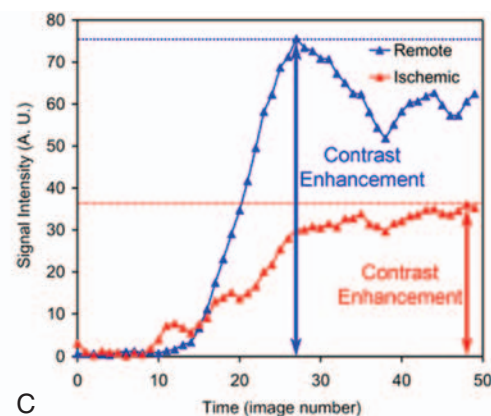
A summary of CMR protocols useful for evaluating patients with various cardiomyopathies is shown in Table 18-e2 (see website). Echocardiography will likely remain the first test for patient evaluation because of its ease of use and widespread availability (see Chap. 15). However, with its multifaceted approach within a study, CMR is considered by many experienced centers to be the best noninvasive diagnostic test for assessing the etiology in patients with a newly diagnosed



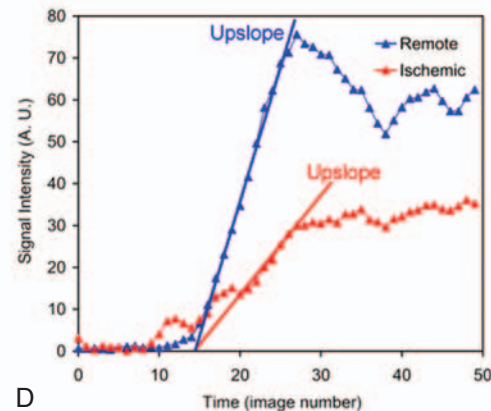
A



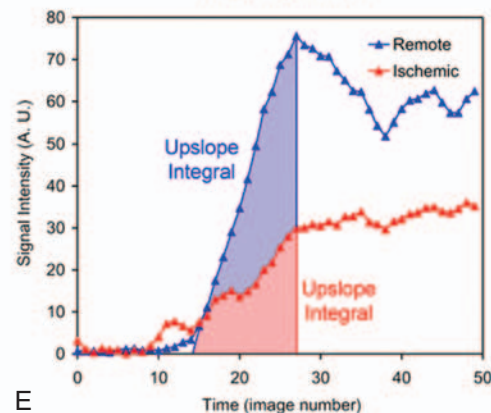
B



C



D



E

FIGURE 18-8 **A**, Qualitative interpretation of a first-pass myocardial perfusion study as a bolus of gadolinium contrast transits through the heart. Note that an anterior subendocardial perfusion defect appears starting at image 18 and persists at peak contrast enhancement (image 26) and later. **B**, Time intensity curves measured from a first-pass CMR perfusion study. The open green circles were measured in the RV cavity. The dark green circles were measured in the LV cavity. The blue triangles were measured in a sector representing normal vasodilated myocardium, and the red triangles came from a region of the myocardium with severely reduced perfusion (anterior subendocardium in this case). **C, D, E**, Methods for semiquantitative analysis of perfusion. Common semiquantitative parameters for measuring myocardial perfusion include peak contrast enhancement (**C**), upslopes of the time-intensity curves (**D**), and upslope integrals (**E**). (Courtesy of Dr. Andrew Arai, National Heart, Lung, and Blood Institute, National Institutes of Health, Bethesda, Md.)

cardiomyopathy (**Fig. 18-9**). Table 18-e3 (see website) summarizes the CMR features—using rest and stress myocardial perfusion, regional function, LGE, and T2-weighted imaging by CMR—for differentiating myocardial viability, ischemia, infarction, and noncoronary causes of cardiomyopathy. When the LGE pattern is used to rule in nonischemic cardiomyopathy, it is important to recognize that infarction can appear nonsubendocardial at the edge of the infarction, or may be a result of microvascular obstruction or endocardial thrombus (both appear dark on LGE imaging), thus mimicking a nonischemic pattern of LGE. Comparing the LGE image against cine gradient echo or perfusion images in matching location or by using a long inversion time (600 milliseconds or longer) can help determine the presence of microvascular obstruction or thrombus.⁶⁰ Tissue tagging may help resolve any

suspected regional wall motion abnormality at rest or stress or when myocardial adhesion from pericardial diseases becomes part of the issue under consideration.

HYPERTROPHIC CARDIOMYOPATHY. CMR cine imaging of LV structure and function and tissue characterization are useful for distinguishing between physiologic and pathologic forms of LV hypertrophy (LVH; see Chap. 69). Olivotto and colleagues⁶¹ have reported that substantial overlap in LV mass index values exists among patients with hypertrophic cardiomyopathy (HCM) and normal control subjects from the Framingham Heart Study, in which at least 20% of HCM patients had a normal LV mass index. Whereas a dichotomous LV mass index cutoff value cannot be used as a diagnostic criterion for HCM,



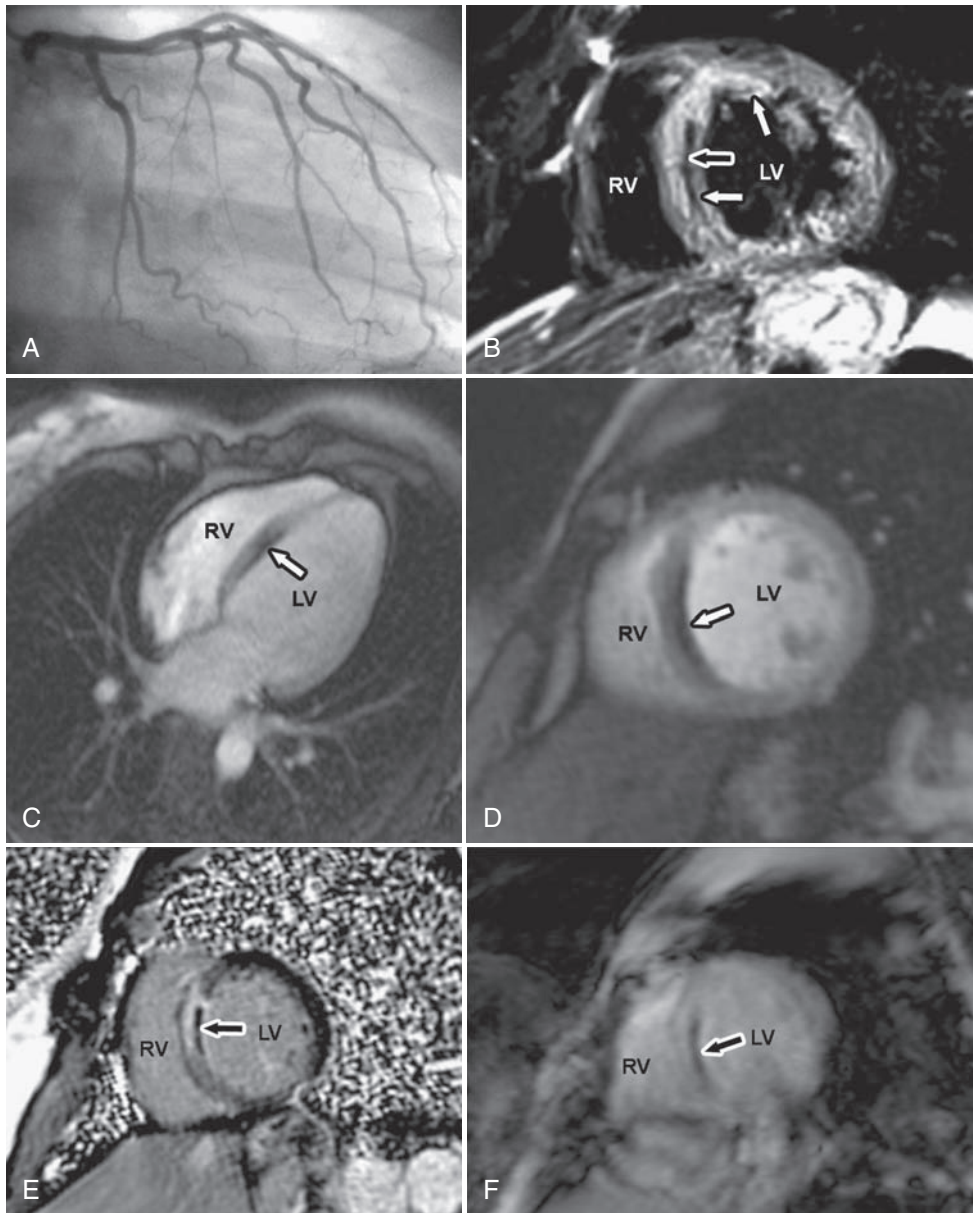


FIGURE 18-9 A 42-year-old woman was admitted with several days of chest pain and found to have transient ST-segment elevation and abnormal serum troponin levels. **A**, Whereas urgent coronary angiography did not reveal any significant coronary stenosis, multimodality CMR provided information that indicated an acute coronary event. **B**, T2-weighted fast spin-echo imaging demonstrated an area of high signal intensity consistent with transmural myocardial edema (area at risk) in the anteroseptal wall (arrows). Although there was no significant epicardial coronary stenosis, evidence of tissue no-reflow was seen in the subendocardium of the anteroseptal wall within the area at risk (black arrow). **C**, On first-pass myocardial perfusion imaging, the no-reflow zone is seen as a dense perfusion defect (**C** and **D**, arrows), and as a dark region within the gadolinium-enhanced area of infarction on late gadolinium enhancement imaging (**E**, arrow). **F**, In addition, very low signal intensity was seen in this region by T2* imaging, raising the suspicion of coexisting intramyocardial hemorrhage (arrow).

Petersen and associates⁶² have observed that an end-diastolic wall thickness-to-cavity volume ratio less than 0.15 mm/mL/m² and lack of LGE of the ventricular myocardium can provide accurate differentiation between physiologic and pathologic LVH. Limited echocardiographic windows lead to obliquity and errors in geometric measurements. Rickers⁶³ has reported that CMR detects hypertrophic segments in 6% of patients in whom it was undetected by two-dimensional echocardiography. In addition, echocardiography underestimated the magnitude of hypertrophy determined by CMR in the basal anterolateral wall by 20% and the presence of extreme hypertrophy (>30-mm wall thickness) by 10%. Both findings have important prognostic implications. For apical hypertrophic cardiomyopathy, CMR

can detect hypertrophied segments of the LV apex not easily identifiable by echocardiography. CMR should also be performed when discrepancy between electrocardiographic and echocardiographic evidence of hypertrophy exists. In HCM patients with severe septal hypertrophy and symptomatic dynamic LV outflow tract obstruction, CMR has advantages over echocardiography in assessing the reduction of septal thickness from surgical myectomy or alcohol septal ablation, which has implications regarding patient symptoms and outcome.⁶⁴

LV mass index varies widely with maximal LV wall thickness because of heterogeneity of the HCM phenotype but has important prognostic implications. A markedly elevated LV mass index (men > 91 g/m²; women > 69 g/m²) was sensitive (100%), whereas maximal wall thickness of more than 30 mm was specific (91%) for cardiac deaths.⁶¹ Other potential markers of adverse prognosis include right ventricular (RV) hypertrophy or myocardial edema by T2-weighted imaging.⁶⁵ Typical patterns of findings in HCM characterized by a multicomponent CMR examination are listed in Table 18-e3 (see website) and illustrated in the case example in **Figure 18-10**. This approach may offer not only accurate HCM diagnosis but also novel understanding of myocardial pathophysiology. Petersen and colleagues⁶⁶ have found that blunted endocardial myocardial blood flow and myocardial fibrosis are both related to the degree of hypertrophy, raising the intriguing possibility that microvascular dysfunction plays an important role in the development of hypertrophy and myocardial fibrosis as a substrate to sudden cardiac death. Long-term prognostic evidence using contrast-enhancing techniques by CMR is currently lacking in HCM patients, but LGE has been associated with ventricular arrhythmias⁶⁷ and progressive ventricular dilation. By its concurrent assessment of altered physiology secondary to coronary microvascular dysfunction, fibrosis, and hypertrophy, CMR will advance the understanding of myocardial substrates and triggers relevant

to sudden cardiac death and guidance of ICD therapy in HCM patients.

ARRHYTHMOGENIC RIGHT VENTRICULAR CARDIOMYOPATHY. Arrhythmogenic RV cardiomyopathy (ARVC; see **Chap. 68**) distinguishes itself from other cardiomyopathies by a predisposition to ventricular arrhythmias that precede overt morphologic abnormalities and even histologic substrate and by diverse phenotypic manifestations, despite success in isolating the causative desmosomal mutations. CMR offers advantages over echocardiography and RV angiography by its quantitative and volumetric assessment of cardiac function and its characterization of myocardial fibrofatty tissue (see **Fig. 68-14**). Recent

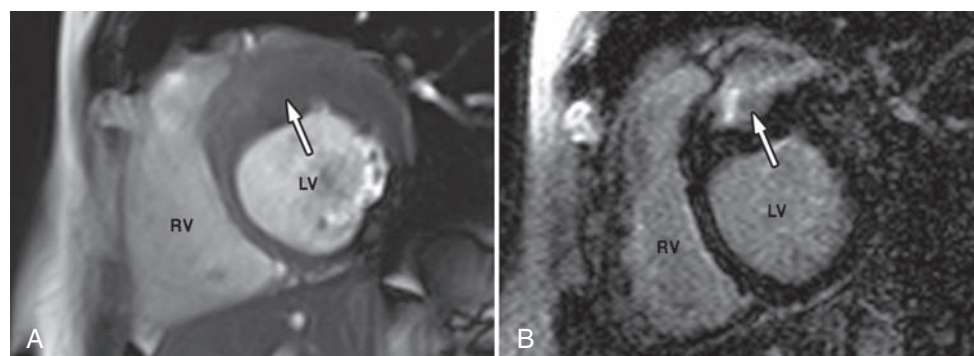


FIGURE 18-10 **A**, Patient with hypertrophic cardiomyopathy with severe panseptal hypertrophy (arrow). **B**, The septum demonstrates dense LGE (arrow) consistent with fibrosis.

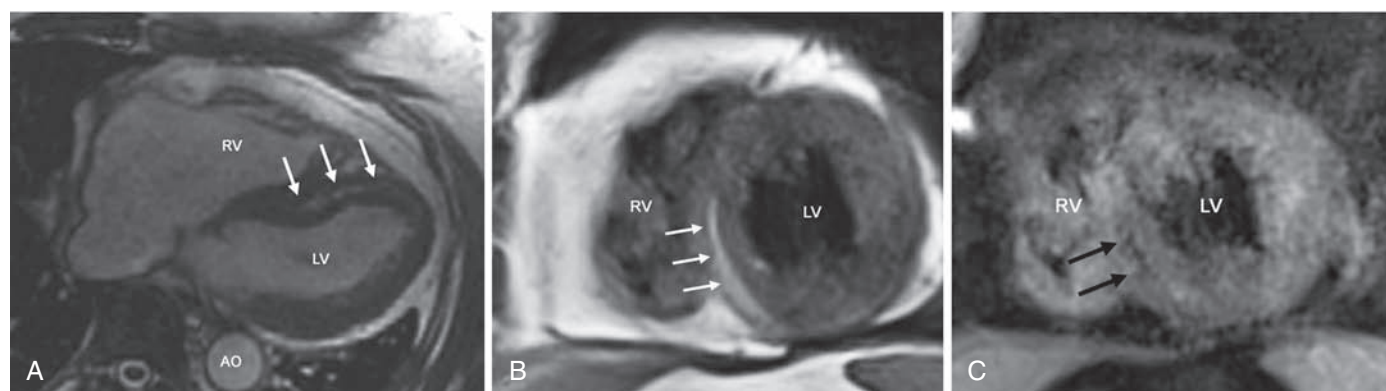


FIGURE 18-11 A 56-year-old woman presenting with recurrent presyncope was found to have nonsustained ventricular tachycardia on Holter monitoring and was referred for CMR assessment. Echocardiography was normal. **A**, Long-axis cine CMR showed an area of high signal (arrows) within the mid to distal interventricular septal wall, representing suspected fatty infiltration. The RV is normal in size, function, and morphology. **B**, Midventricular short-axis T1-weighted FSE CMR confirms a layer of fatty infiltration (arrows) in the matching inferoseptal walls of the LV. **C**, The same short-axis location acquired with a T1-weighted FSE sequence with fat saturation revealed a specific and clear nulling of a layer of fatty infiltration (black arrows).

evidence has indicated that early and predominant LV disease exists in variant groups (**Fig. 18-11**).⁶⁸ Such enthusiasm for CMR for assessing ARVC was somewhat curbed by a lack of standardized imaging protocols in the past and inherent subjectivity in interpreting myocardial fat and wall motion abnormality of the thin-walled crescent-shaped right ventricle.⁶⁹ Recent efforts toward the standardization of CMR protocols have affirmed the value of CMR as an integral component in the workup of ARVC.⁷⁰ Quantitative RV measurements by CMR are accurate and reproducible. Fat-suppressed LGE imaging of the RV myocardium using a short inversion time (<150 milliseconds) has shown high correlation with endomyocardial biopsy and inducibility of ventricular arrhythmias.⁷¹ Fat infiltration of the RV wall as an isolated finding is of limited specificity for diagnosing ARVC. Sen-Chowdhry and associates⁷² have studied 232 patients with suspected to have ARVC using clinical evaluation, genetic analysis, and a dedicated CMR protocol; 134 patients fulfilled the extended diagnostic criteria of ARVC. CMR had a sensitivity of 96% and a specificity of 78% in detecting ARVC. The authors suggested that CMR has the potential to detect patients with early disease not characterized by the task force guideline. Future studies will need to determine the diagnostic and prognostic role of CMR relative to clinical evaluation, genetic analyses, and the new immunohistochemical analysis of plakoglobin signals.⁷³ Jain and coworkers⁷⁴ have provided a current and detailed review of the role of CMR concurrent to the recent expansion of the genetic understanding of ARVC.

MYOCARDITIS. CMR targets three aspects of tissue abnormality in myocarditis—myocardial edema by T2-weighted imaging, regional hyperemia and capillary leak by early gadolinium enhancement ratio (EGE_r), and myocardial necrosis or fibrosis by LGE imaging. Table

18-e1 (see website) summarizes the diagnostic criteria of these techniques for acute myocarditis (see **Chap. 70**). Further details of these diagnostic criteria can be found in a recent expert consensus.⁷⁵ A case example of acute myocarditis is illustrated in **Figure 18-12** (see **Fig. 70-5**). From pooled data of single-center studies, T2-weighted imaging, EGE_r, and LGE have individual sensitivities and specificities of 70% and 71%, 74% and 83%, and 59% and 86%, respectively. An expert panel has suggested that two or more of the three tissue-based criteria provide modest sensitivity (67%) but high specificity (91%) for the diagnosis of myocarditis.⁷⁵ In cases with high index of clinical suspicion but negative CMR tissue findings, a repeat study in a few weeks may be necessary for diagnosis because inflammation may be focal and difficult to detect in the first few days of disease. Early evidence has indicated that a persistence of LGE 4 weeks after symptom onset is predictive of adverse functional and clinical outcomes.⁷⁶

CARDIAC SARCOIDOSIS. CMR techniques and corresponding findings in cardiac sarcoidosis are listed in Tables 18-e2 and 18-e3 (see website), and a case example is shown in **Figure 18-13** (see **Chap. 68**). The CMR techniques described may enhance disease detection through the successive histologic stages of disease: tissue edema, non-caseating granulomatous infiltration, and patchy myocardial fibrosis. Disease activity may explain any discordance between T2-weighted and LGE findings. In 81 patients with extracardiac sarcoidosis, Patel and colleagues⁷⁷ have found that LGE imaging identifies abnormalities consistent with cardiac sarcoidosis in 26% of patients compared with 12% by the modified Japanese Ministry of Health guidelines. LGE-positive patients had a ninefold increase in the hazard of death or major dysrhythmic events requiring intervention. CMR can also be used to guide sampling during endomyocardial biopsy and thus

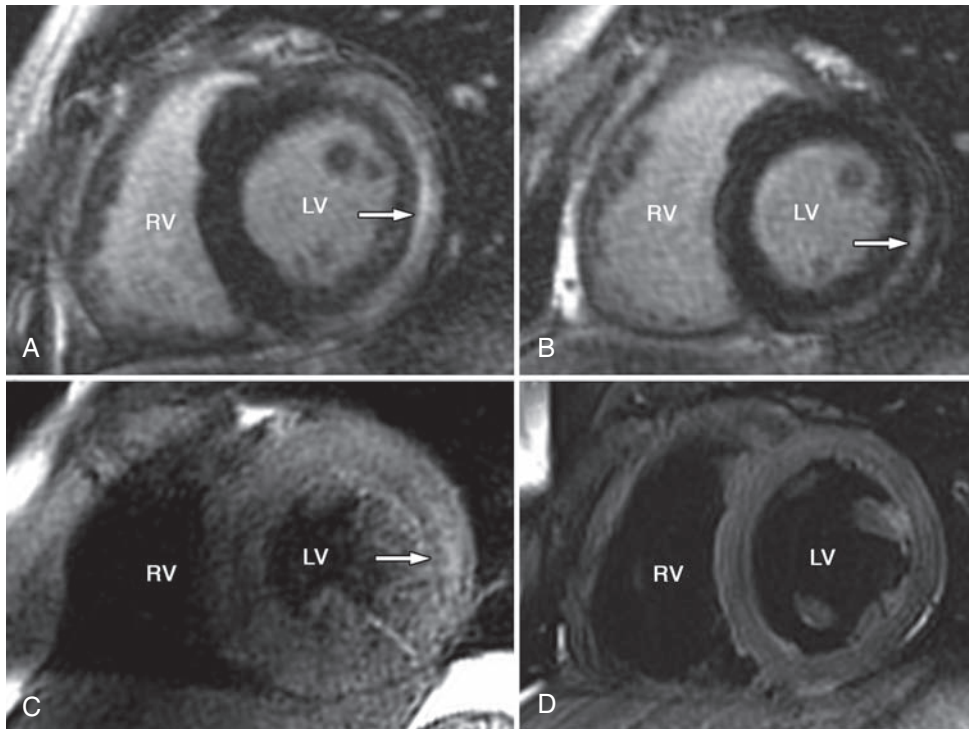


FIGURE 18-12 A 17-year-old college student presented with sudden onset of chest pain and ST-segment elevation in the anterior and anterolateral leads. Urgent coronary angiography revealed no significant coronary arterial stenosis but his serum troponin T level was markedly elevated to 100 times the upper limit of normal within the first 24 hours of presentation, and there was a large region of anterior and anterolateral hypokinesis. CMR performed during the first 48 hours of presentation showed extensive evidence of myocardial inflammation by LGE imaging involving the epicardial aspect of the anterior and anterolateral walls (**A**), which were matched by a high signal intensity region on T2-weighted FSE edema imaging (**C**), consistent with acute viral myocarditis. Parvovirus serology was elevated fivefold. Three months later, regional function completely resolved. There was evidence of a residual epicardial scar by LGE imaging (**B**) but with no evidence of persistent inflammation on T2-weighted edema imaging (**D**).

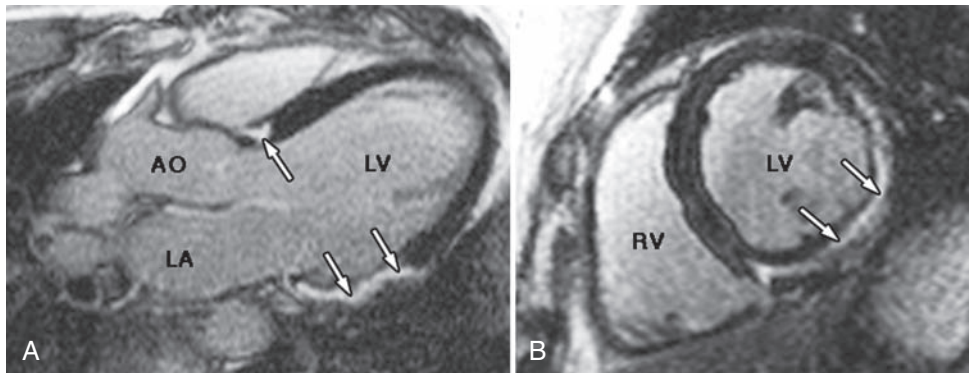


FIGURE 18-13 A 47-year-old man with no prior medical history presented with dizziness and a junctional rhythm with frequent premature ventricular contractions on a resting electrocardiogram. CMR revealed mildly reduced LV systolic function with akinesis of the basal and midinferior and inferolateral walls. LGE images (**A**, long axis; **B**, short axis) demonstrate midmyocardial and epicardial LGE (arrows). In **A**, apart from the inferolateral midwall enhancement (bottom arrows), there was a second focus of LGE seen in the basal septum (top arrow). This pattern of midmyocardial and epicardial LGE is consistent with an infiltrative process, such as sarcoidosis. AO = aorta; LA = left atrium; RV = right ventricle.

increase tissue yield. Despite being reproducible and accurate in reflecting sarcoid progression,⁷⁸ CMR is often currently limited as a monitoring tool for disease progression by a patient's need for an ICD.

CARDIAC AMYLOIDOSIS. The characteristic features of CMR techniques in cardiac amyloidosis are summarized in Table 18-e3 (see website and Chap. 68). Maceira and associates⁷⁹ were the first to report a global subendocardial LGE pattern and an inverse relationship

between endocardial T1 and systemic and myocardial amyloid load. LGE was confirmed to be related to amyloid interstitial expansion in one autopsy case. Furthermore, a transmural T1 gradient across the myocardium minutes after GBCA injection was predictive of cardiac death.⁸⁰ A case example is presented in Figure 18-14.

IDIOPATHIC DILATED CARDIOMYOPATHY. Major advantages of CMR in evaluating suspected idiopathic dilated cardiomyopathy (IDCM) include ruling out ischemic cardiomyopathy, characterizing the pattern of myocardial scar, which has diagnostic and prognostic implications, and monitoring treatment response and disease progression by quantitation of LV structure and function (see Fig. 68-2). In prior studies involving patients with LV dysfunction,⁸¹ LGE was observed in all patients with coronary stenosis, indicating that an ischemic cause of LV dysfunction is unlikely in the absence of LGE. In patients with cardiomyopathy but without angiographic coronary stenosis, 28% had patchy or linear midwall LGE, most often in the basal septum. This LGE pattern consistent with midwall fibrosis has been associated with adverse cardiac events, including sudden death independent of LV structure and function.⁸² This finding is consistent with the postulation that LGE imaging can identify arrhythmogenic substrate. Nazarian and colleagues⁸³ have found that LGE involving 26% to 75% of wall thickness is predictive of the inducibility of ventricular tachycardia, independent of LV ejection fraction.

IRON OVERLOAD CARDIOMYOPATHY.

Iron overload cardiomyopathy is most often the result of repeated blood transfusions, such as in patients with thalassemia major, but can be caused by hereditary hemochromatosis, a genetic disorder caused by mutations of *HFE* or the transferrin receptor gene (see Chap. 68). In patients with transfusion-dependent thalassemia major, premature cardiac death as a result of myocardial iron toxicity occurs in 50% of patients. Serum ferritin and hepatic iron levels do not reflect cardiac iron overload caused by different transport mechanism from the heart, and chelation therapy readily removes iron from the liver. Global LV systolic function is usually preserved, especially in anemic thalassemic patients, until severe

cardiac toxicity occurs, thus providing little if any guidance to chelation therapy, which can potentially reverse this cardiomyopathy. The CMR T2* technique for quantifying myocardial iron is summarized in Table 18-e1 (see website). CMR assessment of myocardial iron overload using T2* quantitation has been responsible for improved delivery of iron chelation therapy⁸⁴ by enabling the development of better chelating agents or treatment intensification. The T2* technique has also been associated with a 70% reduction of iron overload-related mortality in patients with thalassemia major since 2000; further evidence of the prognostic benefit



of T2* was demonstrated in a recent study⁸⁵ of 652 thalassemic patients. Patients with a myocardial T2* shorter than 10 milliseconds had a relative risk of 160 in developing heart failure within 1 year (relative risk further increased to 270 if myocardial T2* was <6 milliseconds; **Fig. 18-15**).

OTHER CARDIOMYOPATHIES

CHAGAS DISEASE. Chagas disease is a myocarditis caused by infection from the protozoan *Trypanosoma cruzi* endemic in Central and South America (see **Chap. 71**), but rare cases have been reported in North America. Although most patients have a self-limiting course once immunity develops within 10 weeks, about 30% of untreated cases will have persistent parasitemia and a latent infection that manifest 10 to 20 years later as a severe dilated cardiomyopathy often associated with ventricular arrhythmias. Once heart failure develops, the 5-year cardiac mortality rate is 50%, and sudden cardiac death is common. Rochitte and associates⁸⁶ have described the typical findings by CMR (see **Table 18-e3** on website) and provided evidence supporting the role of CMR in diagnosing and monitoring patients infected with this disease during the latent period.

NONCOMPACTION. LV noncompaction is a cardiomyopathy characterized by failure of compaction of the trabecular layer (see **Table 18-e3** on website and **Fig. 18-16**; see also **Fig. 26-4**), with a familial pattern reported in approximately 40% of patients. In a cohort-control study, Petersen and coworkers⁸⁷ have reported that a diastolic noncompacted-to-compacted thickness ratio more than 2.3 measured in a long axis is 86% sensitive and 99% specific for diagnosing this condition.

TAKOTSUBO CARDIOMYOPATHY. Transient LV apical ballooning syndrome (or takotsubo cardiomyopathy) is characterized by a transient contractile dysfunction of the LV apex, currently proposed to be caused by high catecholamine levels caused by severe emotional or physical stress (see **Chap. 68**). CMR can be useful for differentiating apical ballooning syndrome from an acute coronary event (see **Table 18-e3** on website and **Fig. 68-5**).⁸⁸ LGE in this setting represents a disproportionate expansion of extracellular matrix with increased collagen I deposition on immunohistochemical tissue staining.⁸⁹

ENDOMYOCARDIAL DISEASE. Endomyocardial disease is a restrictive cardiomyopathy that consists of two variants, endomyocardial fibrosis and Löffler endocarditis. Both are considered the result of direct toxic effects of eosinophils on the myocardium. Hypereosinophilia, regardless of its cause, has been suggested to lead to cardiomyopathy in three stages—necrosis, thrombosis, and fibrosis—although definitive proof in humans is lacking. Hypereosinophilia is the hallmark of Löffler endocarditis whereas it is variable in endomyocardial fibrosis, which has characteristic features on CMR (see **Table 18-e3** on website).

Diastolic Dysfunction

Diastolic function of the left ventricle represents a complex interplay of conditions, including myocardial relaxation, passive ventricular elastic recoil, and pericardial constraints (see **Chaps. 24 and 30**). Similar to other modalities, CMR quantitation of diastolic filling rates and time to peak filling are influenced by the cardiac chronotropic state and left atrial pressure. Phase contrast velocity imaging has been shown to measure mitral inflow and pulmonary venous velocities accurately (validating against Doppler echocardiography; see **Chap. 15**) over a practical scan time of several minutes.⁹⁰ With the advantage of unrestricted scan planes, Paelinck and coworkers⁹¹ have found that early mitral inflow velocity (E) normalized to in vivo mitral septal tissue velocity (Ea) measured using phase contrast CMR provides strong correlation and good agreement with mean pulmonary capillary wedge pressure measured by invasive cardiac catheterization (correlation coefficient = 0.8). CMR-specific tissue grid tagging can determine the rotational and translational motions of the LV myocardium by characterizing the clockwise and anticlockwise rotation at the base and apex during systole, respectively. With adequate temporal

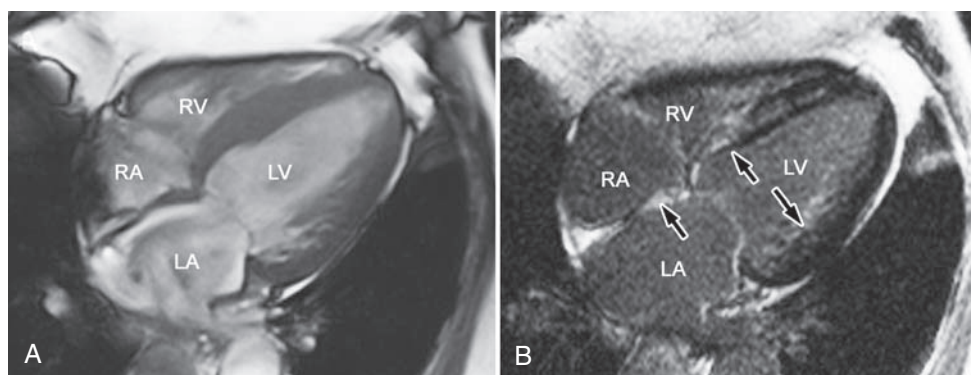


FIGURE 18-14 A 78-year-old man with a history of hypertension and chronic renal insufficiency presented with progressive dyspnea on exertion. **A**, CMR reveals left ventricular hypertrophy with severe biventricular systolic dysfunction (four-chamber long-axis cine systolic image). **B**, Matching LGE imaging shows rapid washout of the contrast agent from the blood pool with diffuse intramyocardial LGE of the septum, subendocardial LGE of the inferior wall, and diffuse atrial LGE (black arrows). This pattern is consistent with amyloidosis.

resolution (less than 35 milliseconds), quantitation of grid distortion permits direct assessment of diastolic intramyocardial deformation measured in strain and strain rates.

Pericardial Disease

At our center, a typical CMR assessment includes cine SSFP imaging, T1- and T2-weighted double-inversion black blood fast spin-echo (FSE; half-Fourier acquisition single-shot turbo spin-echo [HASTE]), and LGE imaging of the whole heart to assess for pericardial changes (see **Chap. 75**). Real-time cine SSFP and phase contrast flow across the tricuspid valve are often added to the examination to enhance the detection of cardiac constriction. First-pass perfusion and pre- and postcontrast T1-weighted techniques (gradient or spin-echo) may also be necessary to determine the vascularity of a pericardial mass (e.g., differentiate tumor from thrombus). Cine myocardial tagged (dark lines or grids) imaging may be useful to identify any perimyocardial adhesion by demonstrating reduced myocardial strain. Single-shot and real-time methods increase the diagnostic yield of the study in patients with irregular heart rhythms, such as atrial fibrillation. A description of our CMR protocol is given in **Table 18-e2** (see website). On T1-weighted FSE imaging, a thickness of up to 3 mm is accepted as normal, accounting for the effects from partial volume averaging, cardiac motion, inclusion of pericardial fluid, and chemical shift artifact. Pericardial sinuses are often mistaken for pathology. The transverse sinus, which lies dorsal to the ascending aorta, and the superior pericardial recess (a curvilinear space to the right of the ascending aorta) may be mistaken for an aortic dissection or a mediastinal mass. The oblique sinus behind the left atrium may be misinterpreted as an esophageal lesion or bronchogenic cyst. Enhancement of the thickened pericardium after the administration of a GBCA suggests active inflammation or pericardial fibrosis (**Fig. 18-17**). CMR is the current test of choice for differentiating constrictive pericarditis from restrictive cardiomyopathy, not only by assessing pericardial thickness but also signs of constrictive physiology. Cardiac CT can demonstrate pericardial calcifications (see **Chap. 19**) but is inferior to CMR because of a lack of assessment of constrictive physiology and hemodynamics and limited tissue characterization.

Pericardial cysts usually have thin smooth walls without internal septa. Their homogeneous transudative contents appear dark on T1-weighted images and bright on T2-weighted images, with no enhancement from GBCA. Proteinaceous cysts appear very bright on T1-weighted images. Pericardial metastases are far more common (from lung, breast, and lymphomas) than primary pericardial tumors (see **Chap. 74**). Malignant invasion of the pericardium often shows focal obliteration of the pericardial line and pericardial effusion. Most neoplasms appear dark or gray on noncontrast T1-weighted images, except metastatic melanoma because of its paramagnetic metals bound by melanin (**Fig. 18-18**). Partial absence of the pericardium is

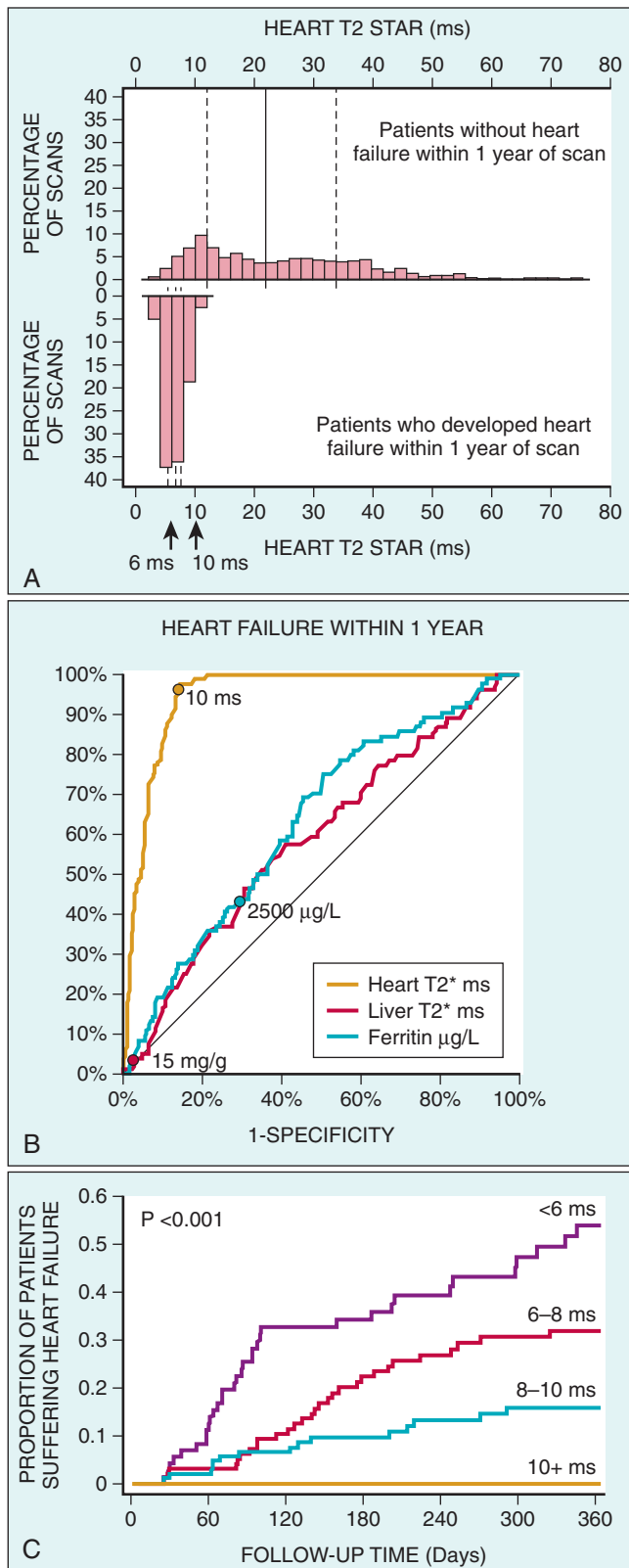


FIGURE 18-15 Outcome of patients with thalassemia major based on CMR imaging. **A**, Frequency distribution of cardiac T2* values in 80 patients who developed heart failure within 1 year of CMR (bottom) versus 572 patients who did not develop heart failure (top). Note the segregation of cardiac T2* in the patients who subsequently developed heart failure into the lowest values; 98% of patients who developed heart failure had a cardiac T2* shorter than 10 milliseconds. The solid vertical black line is the median; dashed black lines are the upper and lower quartiles. **B**, Receiver-operating characteristic curve for the prediction of heart failure within 1 year of CMR. The diagonal line shows the performance of a nondiagnostic test. Although the liver T2* and serum ferritin levels are weakly predictive, the cardiac T2* is greatly superior to both of these conventional measures ($P < 0.001$). The points marked on each line indicate a threshold of 10 milliseconds for cardiac T2*, 0.96 milliseconds for liver T2* (equivalent to 15 mg/kg dry weight), and 2500 µg/L for the serum ferritin level. **C**, Kaplan-Meier curves showing the development of heart failure over 1 year according to baseline cardiac T2* values >10 , 8–10, 6–8, and <6 milliseconds ($P < 0.001$). (From Kirk P, Roughton JB, Porter JM, et al: Cardiac T2* magnetic resonance for prediction of cardiac complications in thalassemia major. *Circulation* 120:1961, 2009.)

usually left-sided and can be associated with atrial septal defect, malformation of the great vessels, patent ductus arteriosus, and defects of the sternum. Rare strangulation of the left atrium through herniation through the pericardial defect is possible. Absence of pericardium is suspected when lung tissue is seen interposed between the aorta and pulmonary artery or between the heart and diaphragm.

Adult Congenital Heart Disease

CMR can provide important diagnostic information beyond echocardiography for the assessment of congenital heart disease (see Chap. 65) based on the following factors: no need for ionizing radiation, three-dimensional tomographic imaging of thoracic structures and anatomy (compared with echocardiographic windows, which are more limited by body growth), and correlation of complex anatomy with blood flow and physiology. This section will focus on CMR assessment of common adult congenital heart diseases.

ATRIAL AND VENTRICULAR SEPTAL DEFECTS. CMR provides a noninvasive alternative to transesophageal echocardiography and even to diagnostic catheterization for assessing patients presenting with right-sided volume overload from a suspected left-to-right shunt. In this situation, a single CMR study can detect the presence of an atrial septal defect (ASD), assess suitability for transcatheter ASD closure (see Chap. 59), quantify right heart size and function by cine SSFP, determine pulmonary-to-systemic shunt ratio (Q_p/Q_s) using velocity-encoded phase contrast, and identify any coexisting anomalous pulmonary venous return using three-dimensional contrast-enhanced MRA. Phase contrast imaging positioned in a plane parallel to the atrial septum and set at a low velocity range (100 cm/sec) can visualize the ASD directly with good correlation with defect size measured invasively.⁹² Phase contrast imaging of tricuspid regurgitation can estimate the pulmonary arterial systolic pressure. Because most closure devices are MRI-compatible, CMR can be used to evaluate residual shunts and proper device deployment. Patients with a ventricular septal defect (VSD) can be assessed using similar CMR techniques. In addition, LGE imaging may help determine whether a VSD has developed as a complication of MI.

ANOMALOUS PULMONARY VENOUS CONNECTION. Using a large field of view, three-dimensional MRA can capture abnormal intrathoracic structures and vascular dynamics in anomalous pulmonary venous return. Near-isotropic in-plane resolution can be achieved allowing reformatting in any plane to detect anomalous venous structures as small as 1 mm (Fig. 18-19). The magnitude of any left-to-right shunt can be assessed by direct blood flow measurements in the anomalous pulmonary vein or by the Q_p/Q_s ratio (see earlier), which is in general more accurate than invasive oximetry measurements caused by the errors from mixed venous return in the right atrium.

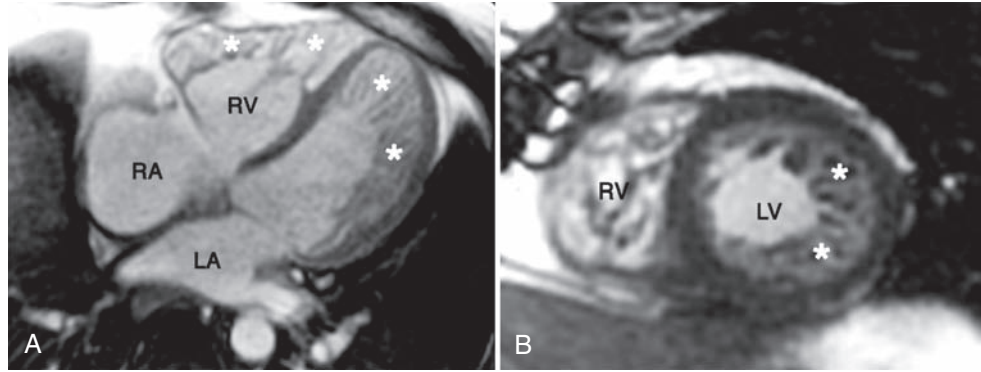


FIGURE 18-16 A 64-year-old man developed decompensated heart failure in the setting of atrial flutter. CMR revealed normal LV size and mild systolic dysfunction (ejection fraction 53%). CMR (**A**, long axis; **B**, short axis) also showed an extensive spongelike appearance of the LV and RV myocardium involving the anterior, lateral, and apical walls (asterisks), consistent with LV noncompaction. The ratio between the noncompacted and compacted myocardium is 9 for the apex and 3 for the lateral wall, values that meet diagnostic criteria for noncompaction.

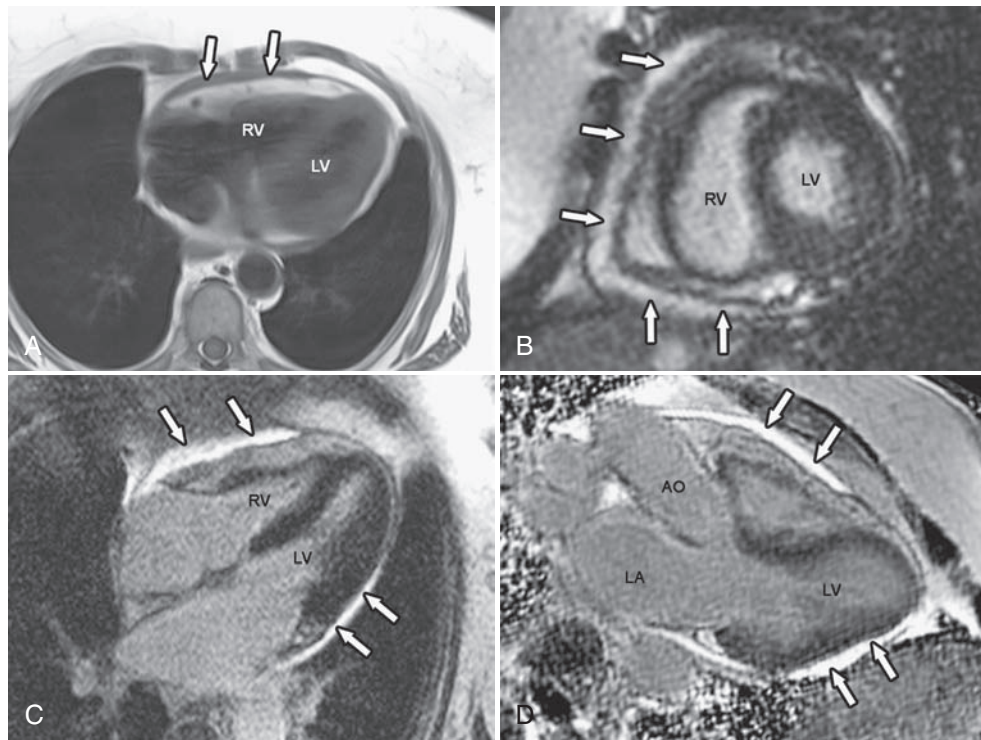


FIGURE 18-17 A 67-year-old man presented with shortness of breath and atypical chest pain. **A**, Double inversion recovery fast spin-echo imaging reveals markedly and diffusely thickened pericardium (arrows). **B, C**, The ventricles are small, whereas the atria are dilated, suggestive of constrictive physiology. With gadolinium contrast, the pericardium demonstrates marked LGE indicative of active and intense pericardial inflammation (**B-D**, arrows).

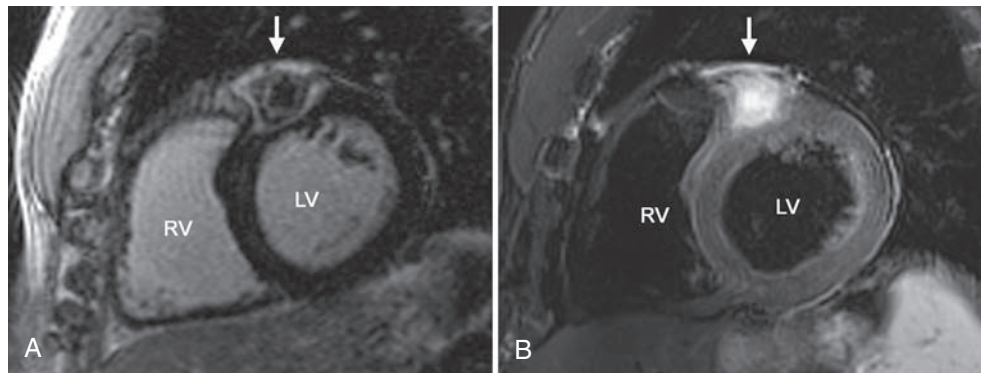


FIGURE 18-18 A 56-year-old man with a history of melanoma with pulmonary metastases presented with a suspicious lesion on a chest CT scan. CMR revealed a 2.4 × 2.2-cm mass in the basal anterior wall of the LV, which was hyperintense on T2-weighted images (**B**), with peripheral late LGE suggestive of tumor necrosis (**A**). These findings are consistent with a focal metastasis of the melanoma to the left ventricle.

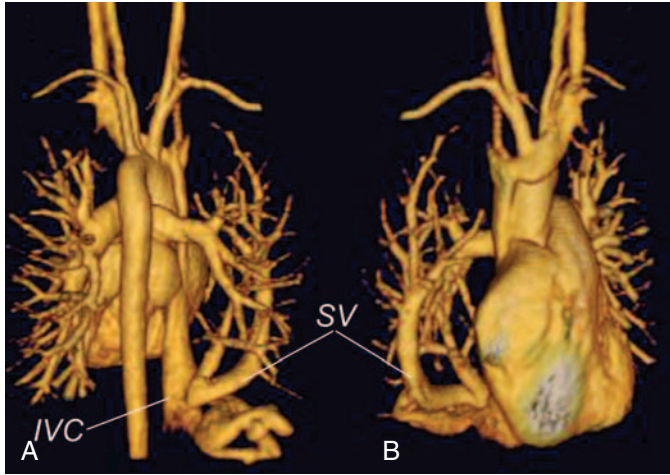


FIGURE 18-19 Posterior (A) and anterior (B) projections of a volume-rendered gadolinium-enhanced three-dimensional magnetic resonance angiogram in a 33-year-old woman with scimitar syndrome. The pulmonary venous return from the right lung drains into the inferior vena cava (IVC) through two veins that form the shape of a Turkish sword, called the scimitar vein (SV). Mesocardia is noted on the anterior projection (B). Because the hemodynamic burden from the left-to-right shunt was relatively small (pulmonary-to-systemic flow ratio measured by phase contrast cine CMR of 1.3), mild right ventricular dilation (end-diastolic volume index, 124 mL/m²; upper limit of normal, 103 mL/m²), normal systolic function, and normal pulmonary artery pressure, no further therapy was recommended. (Courtesy of Dr. Tal Geva, Boston Children's Hospital, Boston.)

COARCTATION OF THE AORTA. Gadolinium-enhanced three-dimensional MRA is sufficient for defining the site of aortic narrowing in most cases (see Figs. 65-33 and 82-4). Cine SSFP, in a long-axis candy cane view, can further delineate the aortic anatomy, degree of obstruction, and aortic valvular dysfunction (caused by a coexisting bicuspid aortic valve). Cine SSFP, in a short-axis stack of the heart, can evaluate LV size, mass, and function, thus assessing the impact of chronic hypertension from aortic coarctation (see Chap. 60). Black blood FSE is useful to evaluate the entire aorta, particularly because it is less affected by metallic artifacts from an implanted endovascular stent than gradient echo techniques. Phase contrast imaging can characterize the descending-to-ascending aorta flow ratio, estimate the pressure gradient across the coarctation, and determine the degree of collateral formation.

CONOTRUNCAL ANOMALIES. Tetralogy of Fallot (TOF) is an increasingly common referral to CMR in young adults. In patients being considered for surgical repair of TOF, key elements in CMR include depiction of all sources of pulmonary blood flow (including pulmonary arterial, aortopulmonary collateral, and ductus-arterial sources) in the presence of RV outflow obstruction, quantitation of the severity of infundibular or pulmonary stenosis, assessment of RV function, and ruling out a coexisting anomalous coronary artery. In patients who have undergone surgery for TOF, CMR attempts to quantify determinants of long-term status, including formation of RV outflow aneurysms, pulmonary regurgitation fraction (especially in patients who underwent patching of the pulmonary valve with postoperative pulmonary regurgitation), biventricular size and global function, and any residual shunt.⁹³ Recently, LGE imaging has been proposed for detection of myocardial fibrosis that has been associated with ventricular dysfunction, exercise intolerance, and arrhythmia.⁹⁴ The principal physiologic abnormality in D-loop transposition of the great arteries (TGA, with D-loop TGA being the most common type) is profound hypoxemia caused by a ventriculoarterial discordant connection, where systemic venous blood flows to the aorta and oxygenated pulmonary venous blood returns to the lung (see Chap. 65). Survival is dependent on systemic-pulmonary circulatory mixing via a ductus arteriosus, ASD, or VSD. The arterial switch operation is now the most common corrective surgery but many adult patients have undergone an atrial switch procedure (Senning or Mustard). CMR is useful for

monitoring these patients after surgical correction by assessing ventricular size and function, flow across the postoperative LV and RV outflow tracts, aortopulmonary collaterals, and other anomalies, such as coarctation of the interrupted aortic arch and pulmonary stenosis.

Valvular Heart Disease

With the capability to assess cardiac structure and function, valvular and great vessel flow hemodynamics, and three-dimensional angiography, CMR can provide complementary information to the echocardiographic evaluation of valvular heart disease (see Chap. 66). Compared with echocardiography, CMR is three-dimensional and does not involve geometric assumption of cardiac shape; thus, it is more sensitive in detecting any change in ventricular sizes, function, and myocardial mass. CMR overcomes the problem of acoustic windows in echocardiography. For aortic stenosis, arbitrary scan plane selection by CMR can visualize and allow direct planimetry of the aortic valve orifice at high spatial resolution. The results of direct planimetry of the aortic valve correlate highly with measures of aortic valve area by transthoracic and transesophageal echocardiography (see Chap. 15), although the reliability of this technique decreases when the aortic valve is heavily calcified, with markedly reduced leaflet motion. Because phase contrast CMR imaging has lower temporal resolution than echocardiography, it may underestimate the peak velocity of blood flow across a highly stenotic aortic valve compared with continuous wave Doppler. A novel application of CMR in identifying vortical blood flow in the main pulmonary artery has been shown to estimate mean pulmonary pressures and differentiate patients with pulmonary hypertension.⁹⁵ The CMR approach to a patient with aortic regurgitation is shown in Figure 18-20. Major limitations that challenge CMR assessment of valve disease are related to irregular heart rhythms, especially atrial fibrillation or frequent ventricular premature contractions. Acquiring phase contrast flow quantitation multiple times and averaging the results may alleviate the error introduced by arrhythmias to some extent, but the results should be interpreted with caution. Most recently, three-dimensional volumetric phase contrast imaging has been developed, which allows visualization of vascular vector flow patterns of large vessels with a novel potential for assessing vascular wall shear stress or ventricular cavity flow dynamics (Fig. 18-21).⁹⁶ This three-dimensional vector flow may allow advancement in the understanding between valvular dysfunction and the progression of the resultant ventricular dysfunction.

Cardiac Thrombi and Masses

Differential diagnoses of an intracardiac mass mainly include thrombus, tumor, or vegetation. LGE imaging can detect thrombus with a higher sensitivity than echocardiography by depicting high contrast between the dark thrombus and its adjacent structures and by imaging in three dimensions. Mural thrombus does not enhance on first-pass perfusion and often has a characteristic etched appearance (black border surrounding a bright center) on LGE imaging, thus providing higher diagnostic specificity than anatomic information alone.⁹⁷ (Fig. 18-22). Weinsaft and colleagues⁶⁰ have demonstrated that setting the inversion time of LGE imaging to 600 milliseconds, which allows recovery of signal in tissues except thrombus, which stays dark, provides a sensitive method for detection of mural thrombus. Microvascular obstruction from MI can be confused with mural thrombus, but it is usually confined within the infarcted myocardium characterized by LGE. Common benign cardiac tumors include atrial myxoma, rhabdomyoma, fibroma, and endocardial fibroelastoma (see Chap. 74). Atrial myxomas are often seen as a round or multilobar mass in the left atrium (75%), right atrium (20%), or ventricles or mixed chambers (5%). It typically has inhomogeneous brightness in the center on cine SSFP imaging because of its gelatinous content and may have a pedunculated attachment to the fossa ovalis. Most malignant cardiac tumors are metastatic and are 20 times more common than primary cardiac malignancies; these include cardiac involvement from direct invasion (lung and breast), lymphatic spread (lymphomas and melanomas), and hematogenous spread (renal cell carcinoma). Cardiac involvement of renal cell carcinoma occurs more often by contiguous spread via the inferior vena cava into the right-sided chambers. Primary cardiac malignancies occur more often in children or young adults; these include angiosarcoma (see Fig. 74-4), fibrosarcoma, rhabdomyosarcoma, and liposarcoma.

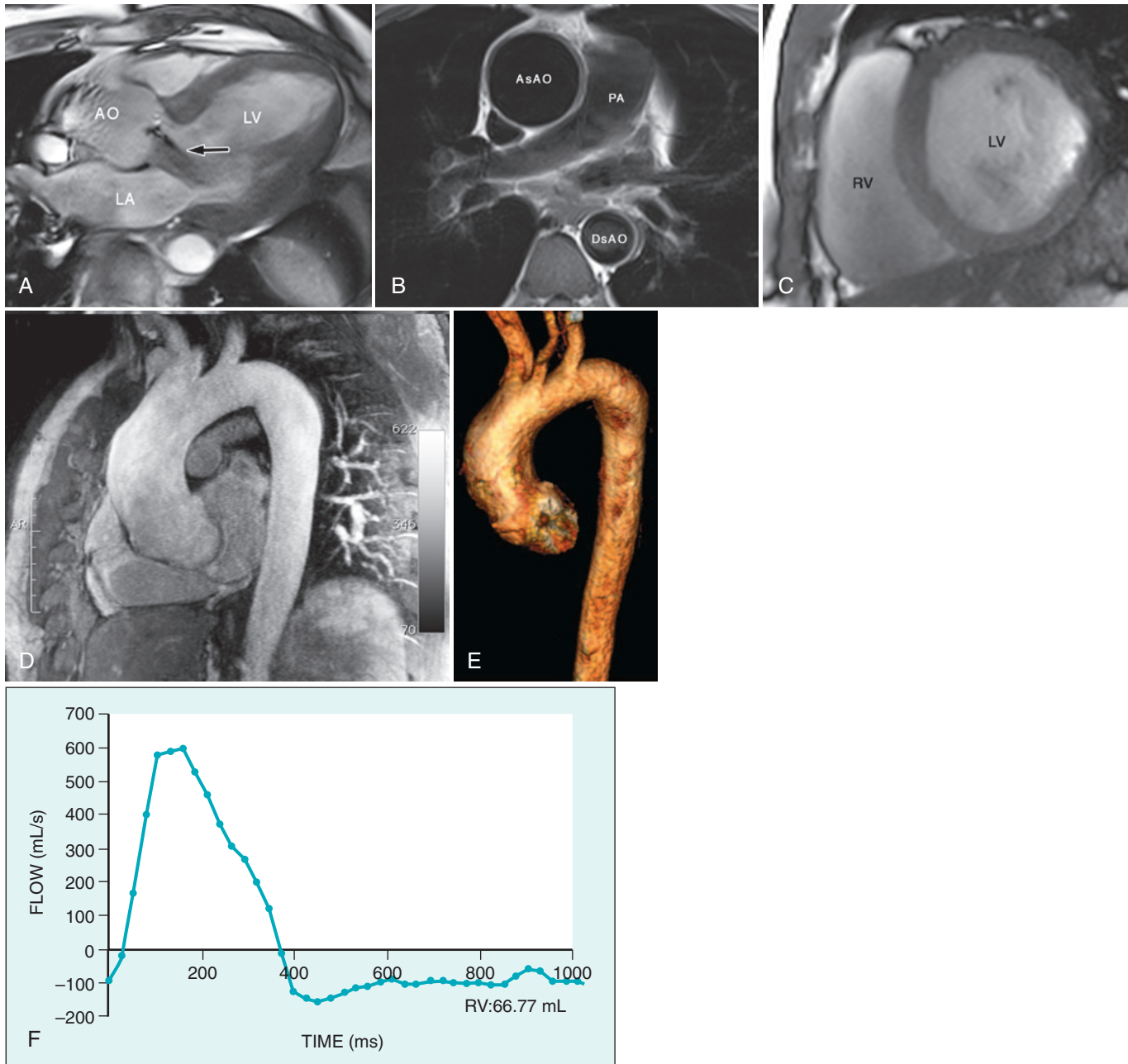


FIGURE 18-20 CMR image of a 67-year-old man with ascending aortic dilation and aortic regurgitation. **A**, Three-chamber cine SSFP showing a dilated LV with an aortic regurgitant jet (black arrow). **B**, Axial T1-weighted double-inversion recovery FSE image demonstrating dilation of the ascending aorta (AsAO). **C**, Short-axis cine CMR demonstrates dilation of the left ventricle. **D**, Maximum intensity projection (MIP) images of gadolinium-enhanced MRA. **E**, Three-dimensional volume reconstruction of gadolinium-enhanced MRA. Note that the AsAO is dilated compared with the descending aorta (DsAO). **F**, Graph of aortic valve flow from phase contrast imaging demonstrates reversal of flow in diastole, consistent with aortic regurgitation, and a calculated regurgitant volume of 66.8 mL. AO = aorta; PA = pulmonary artery; RV = right ventricle.

Novel Cardiac Magnetic Resonance Imaging Techniques

Magnetic Resonance Spectroscopy

Magnetic resonance spectroscopy (MRS) provides information regarding cellular metabolism. Free energy in adenosine triphosphate (ATP) is produced and stored primarily in mitochondria and carried to sites of energy consumption (e.g., myofibrils or ion channels) as phosphocreatine (PCr) through diffusion. Phosphorus-31 MRS assesses energy metabolism and thus the integrity of myocardial cellular functions by

quantifying the concentrations and ratios of PCr and ATP. MRS is currently limited by the low signal-to-noise ratio because of the low concentration of the high-energy phosphate molecules, resulting in a limited sensitivity in detecting viable myocardium and coverage beyond the anterior LV myocardium. However, proton (¹H) MRS has up to a 20-fold improved sensitivity over ³¹P MRS and thus can quantify phosphorylated and unphosphorylated creatine in any part of the LV myocardium.⁹⁸ Using ¹H MRS, a recent study has found that lipid overstorage in human myocytes develops in diabetics in the absence of systolic dysfunction, which may have mechanistic implications for the development of diabetic cardiomyopathy.⁹⁹

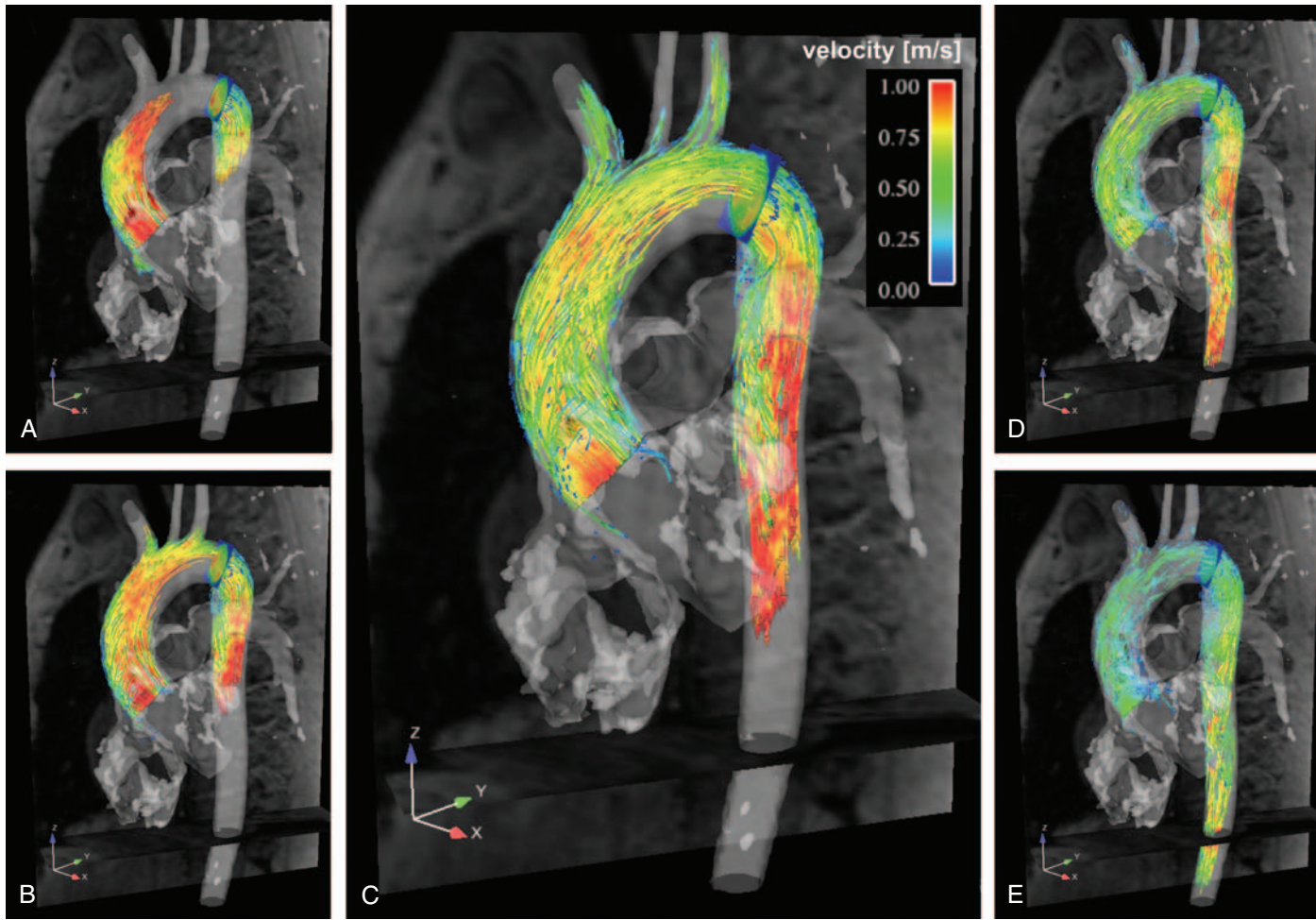


FIGURE 18-21 Time-resolved three-directional three-dimensional velocity-encoded phase contrast MRI of aortic flow. **A-E**, Blood flow visualization using phase contrast angiography (gray shaded isosurface) in combination with time-resolved three-dimensional particle traces in the thoracic aorta depicting the temporal evolution of three-dimensional blood flow in five sequential phases during ventricular systole and early diastole. The individual lines represent traces along the time-resolved velocity vector field and are color-coded according to velocity magnitude in meters per second. (Courtesy of Dr. Michael Markl, University Hospital, Freiburg, Germany.)

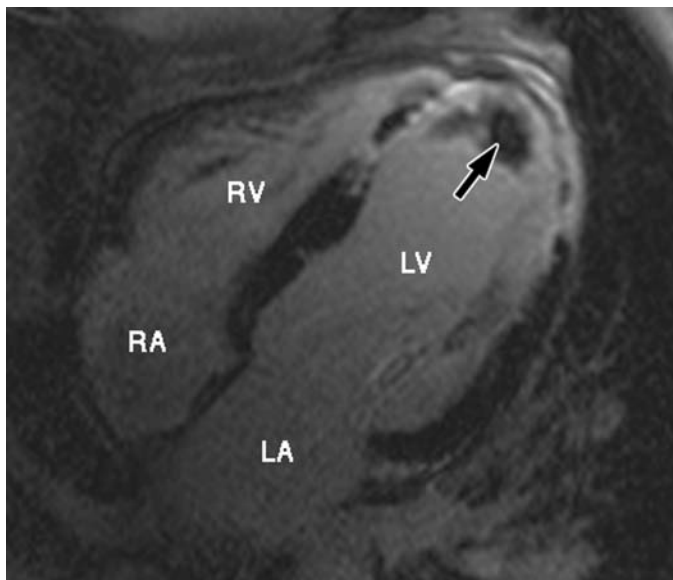


FIGURE 18-22 Characteristic etched appearance of thrombus seen on post-contrast LGE image.

Cardiac Magnetic Resonance at 3 T

Increasing the field strength offers the promise of a higher signal-to-noise-ratio, which indirectly leads to higher image quality, imaging speed, and spatial resolution. T1 of myocardium is lengthened at 3 T and therefore can lead to a higher contrast against blood pool or gadolinium-enhanced regions, because myocardium appears darker as a result of slower T1 signal recovery. This can also reduce the amount of contrast needed to achieve the same level of diagnostic quality in contrast-enhanced techniques. At a diagnostic level, pulse sequences such as myocardial perfusion imaging and LGE imaging are readily improved from the higher signal-to-noise ratio. In the 3-T environment, the benefit of parallel imaging can be used in more applications, thus enhancing sequence efficiency with an acceptable loss of signal-to-noise ratio. Because resonance frequencies of spins in water and fat are more widely separated at 3 T, fat suppression can be more precise, leading to better image quality. T2 and T2* are both shorter, and thus hypointense structures such as blood clots are more easily seen as dark structures at 3 T. The elevated signal-to-noise-ratio also allows novel applications that are limited by low signal at 1.5 T, such as blood oxygen level deoxygenation (BOLD) perfusion and MRS. However, several technical problems exist for CMR at 3 T. RF energy deposition (as measured by specific absorption rate [SAR]) is elevated at 3 T, which can lead to patient or device heating. This can be solved by separating high SAR sequences by breath-holds so that heat dissipation occurs between successive data acquisition. Chemical shift artifacts from adjacent fat and off-resonance artifacts from through-plane blood flow, in addition to SAR limitation, can create severe

artifacts in cine SSFP imaging at 3 T. This problem may be alleviated with resonance frequency tuning techniques.

Molecular Cardiac Magnetic Resonance Imaging

Molecular CMR imaging is currently experimental, but imaging molecular targets can theoretically improve the following: (1) specific disease diagnosis; (2) preclinical or early disease detection and monitoring; (3) treatment response from novel therapies; and (4) patient prognostication.¹⁰⁰ Gadolinium chelates combined with a fibrin-specific peptide ligand have been demonstrated to detect thrombi implanted into the left atrium or pulmonary artery and in vivo coronary thrombus within thrombotic stents.^{101,102} Nanoparticles targeting the adhesion molecule $\alpha_v\beta_3$ -integrin have been used successfully for imaging angiogenesis in experimental atherosclerosis. Ultrasmall USPIO particles accumulate in macrophages in inflamed carotid plaques and have been visualized as dark regions 24 hours after USPIO injection.⁵⁷ Other examples include CMR tracking of intramyocardial transplanted mesenchymal stem cells in an experimental model of MI.¹⁰³ Newer magnetic nanoparticles such as cross-linked iron oxide may improve efficiency in labeling stem cells, with reduced immunogenicity and toxicity.

Future Perspectives

Technologic advances of CMR in the coming years will likely focus on improving the study throughput, protocol consistency, and patient tolerability to CMR examinations. Faster data collection achieved by combining efficient parallel imaging algorithms and improved surface coil elements may reduce or eliminate the need for patient breath-holding and reduce CMR scan time. With more efficient data collection methods, time-resolved techniques such as cine imaging may be replaced by real-time imaging. Three-dimensional pulse sequence techniques or performing CMR at 3 T can offset the reduction in the signal-to-noise ratio caused by data undersampling by parallel imaging. It is therefore conceivable that combinations of these methods will replace the current standard two-dimensional methods. Semiautomated cardiac localization and scanning algorithms will be developed to reduce the time required for training physicians and technologists. New contrast agents hold promise for improving the assessment of myocardial or vascular physiology. For example, a novel contrast agent with perfusion-dependent reversible binding to myocardial collagen might substantially improve the quality of CMR myocardial perfusion imaging and enable the option of performing exercise stress testing before CMR imaging.¹⁰⁴ Blood pool contrast agents may improve the delineation of coronary stenosis by whole-heart coronary MRA and assessment of myocardial perfusion.^{105,106} Although further development is needed in interventional instrumentation and MRI hardware, CMR-guided interventions, especially for electrophysiologic applications, hold promise for improving ablative procedures. Clinical trials involving patients with pacemakers will establish criteria for selected patients to undergo CMR safely.

CMR will likely expand its role in clinical decision making and discovery of new cardiac therapies. The former is supported by the multifaceted approach of CMR in combining information regarding cardiac structure and novel physiology, a growing understanding of CMR technology and its acceptance in the clinical cardiology community, and an increasing awareness of the risk of medical radiation exposure. The latter is evidenced by the high reproducibility of quantitative CMR in reducing study sample sizes and costs required for testing new therapies in clinical trials. Ongoing studies that investigate any cost-benefit improvement by CMR will further define the future directions of CMR as a diagnostic tool.

REFERENCES

Basic Principles and Technical Aspects

1. Wertman R, Altun E, Martin DR, et al: Risk of nephrogenic systemic fibrosis: Evaluation of gadolinium chelate contrast agents at four American universities. *Radiology* 248:799, 2008.

2. Prince MR, Zhang H, Morris M, et al: Incidence of nephrogenic systemic fibrosis at two large medical centers. *Radiology* 248:807, 2008.
3. Kellman P, Arai AE, McVeigh ER, Aletras AH: Phase-sensitive inversion recovery for detecting myocardial infarction using gadolinium-delayed hyperenhancement. *Magn Reson Med* 47:372, 2002.
4. Sievers B, Elliott MD, Hurwitz LM, et al: Rapid detection of myocardial infarction by subsecond, free-breathing delayed contrast-enhancement cardiovascular magnetic resonance. *Circulation* 115:236, 2007.
5. Peters DC, Wylie JV, Hauser TH, et al: Detection of pulmonary vein and left atrial scar after catheter ablation with three-dimensional navigator-gated delayed enhancement MR imaging: Initial experience. *Radiology* 243:690, 2007.
6. Gerber BL, Raman SV, Nayak K, et al: Myocardial first-pass perfusion cardiovascular magnetic resonance: History, theory, and current state of the art. *J Cardiovasc Magn Reson* 10:18, 2008.
7. Cheng AS, Pegg TJ, Karamitsos TD, et al: Cardiovascular magnetic resonance perfusion imaging at 3-tesla for the detection of coronary artery disease: a comparison with 1.5-tesla. *J Am Coll Cardiol* 49:244, 2007.
8. Aletras A: Retrospective determination of the area at risk for reperfused acute myocardial infarction with T2-weighted cardiac magnetic resonance imaging: Histopathological and displacement encoding with stimulated echoes (DENSE) functional validations. *Circulation* 113:1865, 2006.
9. Kellman P, Aletras AH, Mancini C, et al: T2-prepared SSFP improves diagnostic confidence in edema imaging in acute myocardial infarction compared to turbo spin echo. *Magn Reson Med* 57:89, 2007.
10. Aletras AH, Kellman P, Derbyshire JA, Arai AE: ACUT2E TSE-SSFP: A hybrid method for T2-weighted imaging of edema in the heart. *Magn Reson Med* 59:229, 2008.
11. Wood JC, Otto-Duessel M, Aguilar M, et al: Cardiac iron determines cardiac T2*, T2, and T1 in the gerbil model of iron cardiomyopathy. *Circulation* 112:535, 2005.
12. Tanner MA, He T, Westwood MA, et al: Multi-center validation of the transferability of the magnetic resonance T2* technique for the quantification of tissue iron. *Haematologica* 91:1388, 2006.
13. Pennell D: MRI and iron-overload cardiomyopathy in thalassaemia. *Circulation* 113:43, 2006.
14. Pennell DJ: T2* magnetic resonance and myocardial iron in thalassaemia. *Ann N Y Acad Sci* 1054:373, 2005.
15. Bluemke DA, Achenbach S, Budoff M, et al: Noninvasive coronary artery imaging: Magnetic resonance angiography and multidetector computed tomography angiography: A scientific statement from the American Heart Association Committee on Cardiovascular Imaging and Intervention of the Council on Cardiovascular Radiology and Intervention, and the Councils on Clinical Cardiology and Cardiovascular Disease in the Young. *Circulation* 118:586, 2008.
16. Manning WJ, Nezafat R, Appelbaum E, et al: Coronary magnetic resonance imaging. *Magn Reson Imaging Clin N Am* 15:609, 2007.
17. Yang Q, Li K, Liu X, et al: Contrast-enhanced whole-heart coronary magnetic resonance angiography at 3.0-T: A comparative study with X-ray angiography in a single center. *J Am Coll Cardiol* 54:69, 2009.

Patient Safety

18. Nazarian S, Halperin H: How to perform magnetic resonance imaging on patients with implantable cardiac arrhythmia devices. *Heart Rhythm* 6:138, 2009.
19. Roguin A, Schwitzer J, Vahlhaus C, et al: Magnetic resonance imaging in individuals with cardiovascular implantable electronic devices. *Europace* 10:336, 2008.
20. Nazarian S, Roguin A, Zviman MM, et al: Clinical utility and safety of a protocol for noncardiac and cardiac magnetic resonance imaging of patients with permanent pacemakers and implantable-cardioverter defibrillators at 1.5 tesla. *Circulation* 114:1277, 2006.

Standards

21. Kramer CM, Barkhausen J, Flamm SD, et al: Standardized cardiovascular magnetic resonance imaging (CMR) protocols, society for cardiovascular magnetic resonance: Board of trustees task force on standardized protocols. *J Cardiovasc Magn Reson* 10:35, 2008.
22. Hundley WG, Bluemke D, Bogaert JG, et al: Society for Cardiovascular Magnetic Resonance guidelines for reporting cardiovascular magnetic resonance examinations. *J Cardiovasc Magn Reson* 11:5, 2009.

Coronary Artery Disease

23. Kim RJ, Shah DJ: Fundamental concepts in myocardial viability assessment revisited: When knowing how much is "alive" is not enough. *Heart* 90:137, 2004.
24. Hsu LY, Natanzon A, Kellman P, et al: Quantitative myocardial infarction on delayed enhancement MRI. Part I: Animal validation of an automated feature analysis and combined thresholding infarct sizing algorithm. *J Magn Reson Imaging* 23:298, 2006.
25. Kim RJ, Albert TS, Wible JH, et al: Performance of delayed-enhancement magnetic resonance imaging with gadoversetamide contrast for the detection and assessment of myocardial infarction: An international, multicenter, double-blinded, randomized trial. *Circulation* 117:629, 2008.
26. Ganame J, Messalli G, Dymarkowski S, et al: Impact of myocardial haemorrhage on left ventricular function and remodelling in patients with reperfused acute myocardial infarction. *Eur Heart J* 30:1440, 2009.
27. Ricciardi MJ, Wu E, Davidson CJ, et al: Visualization of discrete microinfarction after percutaneous coronary intervention associated with mild creatine kinase-MB elevation. *Circulation* 103:2780, 2001.
28. Kwong RY, Chan AK, Brown KA, et al: Impact of unrecognized myocardial scar detected by cardiac magnetic resonance imaging on event-free survival in patients presenting with signs or symptoms of coronary artery disease. *Circulation* 113:2733, 2006.
29. Kwong RY, Sattar H, Wu H, et al: Incidence and prognostic implication of unrecognized myocardial scar characterized by cardiac magnetic resonance in diabetic patients without clinical evidence of myocardial infarction. *Circulation* 118:1011, 2008.
30. Cheong BY, Muthupillai R, Wilson JM, et al: Prognostic significance of delayed-enhancement magnetic resonance imaging: Survival of 857 patients with and without left ventricular dysfunction. *Circulation* 120:2069, 2009.





31. Kwon DH, Halley CM, Carrigan TP, et al: Extent of left ventricular scar predicts outcomes in ischemic cardiomyopathy patients with significantly reduced systolic function: A delayed hyperenhancement cardiac magnetic resonance study. *J Am Coll Cardiol Img* 2:34, 2009.
32. Schmidt A, Azevedo CF, Cheng A, et al: Infarct tissue heterogeneity by magnetic resonance imaging identifies enhanced cardiac arrhythmia susceptibility in patients with left ventricular dysfunction. *Circulation* 115:2006, 2007.
33. Roes SD, Borleffs CJ, van der Geest RJ, et al: Infarct tissue heterogeneity assessed with contrast-enhanced MRI predicts spontaneous ventricular arrhythmia in patients with ischemic cardiomyopathy and implantable cardioverter-defibrillator. *Circ Cardiovasc Imaging* 2:183, 2009.
34. Yan AT, Shayne AJ, Brown KA, et al: Characterization of the peri-infarct zone by contrast-enhanced cardiac magnetic resonance imaging is a powerful predictor of post-myocardial infarction mortality. *Circulation* 114:32, 2006.
35. Kim RJ, Wu E, Rafael A, et al: The use of contrast-enhanced magnetic resonance imaging to identify reversible myocardial dysfunction. *N Engl J Med* 343:1445, 2000.
36. Wellnhofer E, Olariu A, Klein C, et al: Magnetic resonance low-dose dobutamine test is superior to SCAR quantification for the prediction of functional recovery. *Circulation* 109:2172, 2004.
37. Ingkanisorn WP, Kwong RY, Bohme NS, et al: Prognosis of negative adenosine stress magnetic resonance in patients presenting to an emergency department with chest pain. *J Am Coll Cardiol* 47:1427, 2006.
38. Lockie T, Nagel E, Redwood S, Plein S: Use of cardiovascular magnetic resonance imaging in acute coronary syndromes. *Circulation* 119:1671, 2009.
39. Abdel-Aty H, Zagrosek A, Schulz-Menger J, et al: Delayed enhancement and T2-weighted cardiovascular magnetic resonance imaging differentiate acute from chronic myocardial infarction. *Circulation* 109:2411, 2004.
40. Cury RC, Shash K, Nagurney JT, et al: Cardiac magnetic resonance with T2-weighted imaging improves detection of patients with acute coronary syndrome in the emergency department. *Circulation* 118:837, 2008.
41. Codreanu A, Djaballah W, Angioi M, et al: Detection of myocarditis by contrast-enhanced MRI in patients presenting with acute coronary syndrome but no coronary stenosis. *J Magn Reson Imaging* 25:957, 2007.
42. Assomull RG, Lyne JC, Keenan N, et al: The role of cardiovascular magnetic resonance in patients presenting with chest pain, raised troponin, and unobstructed coronary arteries. *Eur Heart J* 28:1242, 2007.
43. Laissy JP, Hyafil F, Feldman LJ, et al: Differentiating acute myocardial infarction from myocarditis: Diagnostic value of early- and delayed-perfusion cardiac MR imaging. *Radiology* 237:75, 2005.
44. Klem I, Heitner JF, Shah DJ, et al: Improved detection of coronary artery disease by stress perfusion cardiovascular magnetic resonance with the use of delayed enhancement infarction imaging. *J Am Coll Cardiol* 47:1630, 2006.
45. Plein S, Ridgway JP, Jones TR, et al: Coronary artery disease: Assessment with a comprehensive MR imaging protocol—initial results. *Radiology* 225:300, 2002.
46. Lee DC, Simonetti OP, Harris KR, et al: Magnetic resonance versus radionuclide pharmacological stress perfusion imaging for flow-limiting stenoses of varying severity. *Circulation* 110:58, 2004.
- 46a. Schwitler J, Wacker CM, van Rossum AC, et al: MR-IMPACT: comparison of perfusion-cardiac magnetic resonance with single-photon emission tomography for the detection of coronary artery disease in a multicentre, multivendor, randomized trial. *Eur Heart J* 29:480, 2009.
47. Wahl A, Paetsch I, Roethemeyer S, et al: High-dose dobutamine-atropine stress cardiovascular MR imaging after coronary revascularization in patients with wall motion abnormalities at rest. *Radiology* 233:210, 2004.
48. Gebker R, Jahnke C, Manka R, et al: Additional value of myocardial perfusion imaging during dobutamine stress magnetic resonance for the assessment of coronary artery disease. *Circ Cardiovasc Imaging* 1:122, 2008.
49. Jahnke C, Nagel E, Gebker R, et al: Prognostic value of cardiac magnetic resonance stress tests: Adenosine stress perfusion and dobutamine stress wall motion imaging. *Circulation* 115:1769, 2007.
50. Steel K, Broderick R, Gandla V, et al: Complementary prognostic values of stress myocardial perfusion and late gadolinium enhancement imaging by cardiac magnetic resonance in patients with known or suspected coronary artery disease. *Circulation* 120:1390, 2009.
51. Doesch C, Seeger A, Doering J, et al: Risk stratification by adenosine stress cardiac magnetic resonance in patients with coronary artery stenoses of intermediate angiographic severity. *J Am Coll Cardiol Img* 2:424, 2009.
52. Dall'Armellina E, Morgan TM, Mandapaka S, et al: Prediction of cardiac events in patients with reduced left ventricular ejection fraction with dobutamine cardiovascular magnetic resonance assessment of wall motion score index. *J Am Coll Cardiol* 52:279, 2008.
53. Wallace EL, Morgan TM, Walsh TF, et al: Dobutamine cardiac magnetic resonance results predict cardiac prognosis in women with known or suspected ischemic heart disease. *J Am Coll Cardiol Img* 2:299, 2008.
54. Yuan C, Kerwin WS: MRI of atherosclerosis. *J Magn Reson Imaging* 19:710, 2004.
55. Kerwin WS, O'Brien KD, Ferguson MS, et al: Inflammation in carotid atherosclerotic plaque: A dynamic contrast-enhanced MR imaging study. *Radiology* 241:459, 2006.
56. Yuan C, Kerwin WS, Yarnykh VL, et al: MRI of atherosclerosis in clinical trials. *NMR Biomed* 19:636, 2006.
57. Trivedi RA, Mallawarachi C, U-King-Im JM, et al: Identifying inflamed carotid plaques using in vivo USPIO-enhanced MR imaging to label plaque macrophages. *Arterioscler Thromb Vasc Biol* 26:1601, 2006.
58. Larose E, Yeghiazarians Y, Libby P, et al: Characterization of human atherosclerotic plaques by intravascular magnetic resonance imaging. *Circulation* 112:2324, 2005.
59. Botnar RM, Perez AS, Witte S, et al: In vivo molecular imaging of acute and subacute thrombosis using a fibrin-binding magnetic resonance imaging contrast agent. *Circulation* 109:2023, 2004.
60. Weinsaft JW, Kim HW, Shah DJ, et al: Detection of left ventricular thrombus by delayed-enhancement cardiovascular magnetic resonance prevalence and markers in patients with systolic dysfunction. *J Am Coll Cardiol* 52:148, 2008.
61. Olivetto I, Maron MS, Autore C, et al: Assessment and significance of left ventricular mass by cardiovascular magnetic resonance in hypertrophic cardiomyopathy. *J Am Coll Cardiol* 52:559, 2008.
62. Petersen SE, Selvanayagam JB, Francis JM, et al: Differentiation of athlete's heart from pathological forms of cardiac hypertrophy by means of geometric indices derived from cardiovascular magnetic resonance. *J Cardiovasc Magn Reson* 7:551, 2005.
63. Rickers C: Utility of cardiac magnetic resonance imaging in the diagnosis of hypertrophic cardiomyopathy. *Circulation* 112:855, 2005.
64. Valeti U, Nishimura R, Holmes D, et al: Comparison of surgical septal myectomy and alcohol septal ablation with cardiac magnetic resonance imaging in patients with hypertrophic obstructive cardiomyopathy. *J Am Coll Cardiol* 49:350, 2007.
65. Abdel-Aty H, Cocker M, Strohm O, et al: Abnormalities in T2-weighted cardiovascular magnetic resonance images of hypertrophic cardiomyopathy: Regional distribution and relation to late gadolinium enhancement and severity of hypertrophy. *J Magn Reson Imaging* 28:242, 2008.
66. Petersen SE, Jerosch-Herold M, Hudsmith LE, et al: Evidence for microvascular dysfunction in hypertrophic cardiomyopathy: New insights from multiparametric magnetic resonance imaging. *Circulation* 115:2418, 2007.
67. Adabag AS, Maron BJ, Appelbaum E, et al: Occurrence and frequency of arrhythmias in hypertrophic cardiomyopathy in relation to delayed enhancement on cardiovascular magnetic resonance. *J Am Coll Cardiol* 51:1369, 2008.
68. Sen-Chowdhry S, Syrris P, Ward D, et al: Clinical and genetic characterization of families with arrhythmogenic right ventricular dysplasia/cardiomyopathy provides novel insights into patterns of disease expression. *Circulation* 115:1710, 2007.
69. Sen-Chowdhry S, McKenna WJ: The utility of magnetic resonance imaging in the evaluation of arrhythmogenic right ventricular cardiomyopathy. *Curr Opin Cardiol* 23:38, 2008.
70. Tandri H, Castillo E, Ferrari VA, et al: Magnetic resonance imaging of arrhythmogenic right ventricular dysplasia: Sensitivity, specificity, and observer variability of fat detection versus functional analysis of the right ventricle. *J Am Coll Cardiol* 48:2277, 2006.
71. Tandri H, Saranathan M, Rodriguez ER, et al: Noninvasive detection of myocardial fibrosis in arrhythmogenic right ventricular cardiomyopathy using delayed-enhancement magnetic resonance imaging. *J Am Coll Cardiol* 45:98, 2005.
72. Sen-Chowdhry S, Prasad SK, Syrris P, et al: Cardiovascular magnetic resonance in arrhythmogenic right ventricular cardiomyopathy revisited: Comparison with task force criteria and genotype. *J Am Coll Cardiol* 48:2132, 2006.
73. Asimaki A, Tandri H, Huang H, et al: A new diagnostic test for arrhythmogenic right ventricular cardiomyopathy. *N Engl J Med* 360:1075, 2009.
74. Jain A, Tandri H, Calkins H, Bluemke DA: Role of cardiovascular magnetic resonance imaging in arrhythmogenic right ventricular dysplasia. *J Cardiovasc Magn Reson* 10:32, 2008.
75. Friedrich MG, Sechtem U, Schulz-Menger J, et al: Cardiovascular magnetic resonance in myocarditis: A JACC White Paper. *J Am Coll Cardiol* 53:1475, 2009.
76. Wagner A, Schulz-Menger J, Dietz R, Friedrich MG: Long-term follow-up of patients paragraph sign with acute myocarditis by magnetic paragraph sign resonance imaging. *MAGMA* 16:17, 2003.
77. Patel MR, Crawley PJ, Heitner JF, et al: Detection of myocardial damage in patients with sarcoidosis. *Circulation* 120:1969, 2009.
78. Vignaux O, Dhote R, Duboc D, et al: Clinical significance of myocardial magnetic resonance abnormalities in patients with sarcoidosis: A 1-year follow-up study. *Chest* 122:1895, 2002.
79. Maceira AM, Joshi J, Prasad SK, et al: Cardiovascular magnetic resonance in cardiac amyloidosis. *Circulation* 111:186, 2005.
80. Maceira AM, Prasad SK, Hawkins PN, et al: Cardiovascular magnetic resonance and prognosis in cardiac amyloidosis. *J Cardiovasc Magn Reson* 10:54, 2008.
81. Senthilkumar A, Majmudar MD, Shenoy C, et al: Identifying the etiology: A systematic approach using delayed-enhancement cardiovascular magnetic resonance. *Heart Fail Clin* 5:349, 2009.
82. Assomull RG, Prasad SK, Lyne J, et al: Cardiovascular magnetic resonance, fibrosis, and prognosis in dilated cardiomyopathy. *J Am Coll Cardiol* 48:1977, 2006.
83. Nazarian S, Bluemke DA, Lardo AC, et al: Magnetic resonance assessment of the substrate for inducible ventricular tachycardia in nonischemic cardiomyopathy. *Circulation* 112:2821, 2005.
84. Tanner MA, Galanello R, Dessi C, et al: A randomized, placebo-controlled, double-blind trial of the effect of combined therapy with deferoxamine and deferiprone on myocardial iron in thalassemia major using cardiovascular magnetic resonance. *Circulation* 115:1876, 2007.
85. Modell B, Khan M, Darlison M, et al: Improved survival of thalassaemia major in the UK and relation to T2* cardiovascular magnetic resonance. *J Cardiovasc Magn Reson* 10:42, 2008.
86. Rochitte CE, Oliveira PF, Andrade JM, et al: Myocardial delayed enhancement by magnetic resonance imaging in patients with Chagas' disease: A marker of disease severity. *J Am Coll Cardiol* 46:1553, 2005.
87. Petersen SE, Selvanayagam JB, Wiesmann F, et al: Left ventricular non-compaction: insights from cardiovascular magnetic resonance imaging. *J Am Coll Cardiol* 46:101, 2005.
88. Wittstein IS, Thiemann DR, Lima JA, et al: Neurohumoral features of myocardial stunning due to sudden emotional stress. *N Engl J Med* 352:539, 2005.
89. Rolf A, Nef HM, Mollmann H, et al: Immunohistological basis of the late gadolinium enhancement phenomenon in tako-tsubo cardiomyopathy. *Eur Heart J* 30:1635, 2009.

Other Clinical Applications

90. Rathi VK, Doyle M, Yamrozik J, et al: Routine evaluation of left ventricular diastolic function by cardiovascular magnetic resonance: A practical approach. *J Cardiovasc Magn Reson* 10:36, 2008.
91. Paelinck BP, de Roos A, Bax JJ, et al: Feasibility of tissue magnetic resonance imaging: A pilot study in comparison with tissue Doppler imaging and invasive measurement. *J Am Coll Cardiol* 45:1109, 2005.
92. Durongpisitkul K, Tang NL, Soongswang J, et al: Predictors of successful transcatheter closure of atrial septal defect by cardiac magnetic resonance imaging. *Pediatr Cardiol* 25:124, 2004.
93. Knauth AL, Gauvreau K, Powell AJ, et al: Ventricular size and function assessed by cardiac MRI predict major adverse clinical outcomes late after tetralogy of Fallot repair. *Heart* 94:211, 2008.
94. Wald RM, Haber I, Wald R, et al: Effects of regional dysfunction and late gadolinium enhancement on global right ventricular function and exercise capacity in patients with repaired tetralogy of Fallot. *Circulation* 119:1370, 2009.

Cardiomyopathies

60. Weinsaft JW, Kim HW, Shah DJ, et al: Detection of left ventricular thrombus by delayed-enhancement cardiovascular magnetic resonance prevalence and markers in patients with systolic dysfunction. *J Am Coll Cardiol* 52:148, 2008.

95. Reiter G, Reiter U, Kovacs G, et al: Magnetic resonance-derived 3-dimensional blood flow patterns in the main pulmonary artery as a marker of pulmonary hypertension and a measure of elevated mean pulmonary arterial pressure. *Circ Cardiovasc Imaging* 1:23, 2008.
96. Frydrychowicz A, Stalder AF, Russe MF, et al: Three-dimensional analysis of segmental wall shear stress in the aorta by flow-sensitive four-dimensional-MRI. *J Magn Reson Imaging* 30:77, 2009.
97. Grizzard JD: Magnetic resonance imaging of pericardial disease and intracardiac thrombus. *Heart Fail Clin* 5:401, 2009.

Novel Techniques

98. Horn M: Cardiac magnetic resonance spectroscopy: A window for studying physiology. *Methods Mol Med* 224:225, 2006.
99. McGavock JM, Lingvay I, Zib I, et al: Cardiac steatosis in diabetes mellitus: A 1H-magnetic resonance spectroscopy study. *Circulation* 116:1170, 2007.
100. Jaffer FA, Weissleder R: Seeing within: Molecular imaging of the cardiovascular system. *Circ Res* 94:433, 2004.

101. Spuentrup E, Buecker A, Katoh M, et al: Molecular magnetic resonance imaging of coronary thrombosis and pulmonary emboli with a novel fibrin-targeted contrast agent. *Circulation* 111:1377, 2005.
102. Botnar RM, Buecker A, Wiethoff AJ, et al: In vivo magnetic resonance imaging of coronary thrombosis using a fibrin-binding molecular magnetic resonance contrast agent. *Circulation* 110:1463, 2004.
103. Kraitchman DL, Gilson WD, Lorenz CH: Stem cell therapy: MRI guidance and monitoring. *J Magn Reson Imaging* 27:299, 2008.
104. Spuentrup E, Ruhl KM, Botnar RM, et al: Molecular magnetic resonance imaging of myocardial perfusion with EP-3600, a collagen-specific contrast agent: Initial feasibility study in a swine model. *Circulation* 119:1768, 2009.
105. Tang L, Merkle N, Schar M, et al: Volume-targeted and whole-heart coronary magnetic resonance angiography using an intravascular contrast agent. *J Magn Reson Imaging* 30:1191, 2009.
106. Paetsch I, Huber ME, Bornstedt A, et al: Improved three-dimensional free-breathing coronary magnetic resonance angiography using gadocoletic acid (B-22956) for intravascular contrast enhancement. *J Magn Reson Imaging* 20:288, 2004.

APPROPRIATE USE CRITERIA RAYMOND Y. KWONG

Cardiovascular Magnetic Resonance

The explosive growth in cardiovascular imaging has sometimes outpaced the evidence on which the use of new technologies should be based. In an effort to guide rational use of these technologies, eight scientific organizations—American College of Cardiology Foundation, American College of Radiology, Society of Cardiovascular Computed Tomography, Society for Cardiovascular Magnetic Resonance, American Society of Nuclear Cardiology, North American Society for Cardiac Imaging, Society for Cardiovascular Angiography and Interventions, and Society of Interventional Radiology—have embarked on a process to determine the appropriateness of selected indications for cardiovascular imaging procedures.

Panelists rated 33 indications for cardiovascular magnetic resonance (CMR) imaging as appropriate (7 to 9 points), uncertain (4 to 6 points), and inappropriate (1 to 3 points), based on the following definition of appropriateness¹:

An appropriate imaging study is one in which the expected incremental information, combined with clinical judgment, exceeds the expected

negative consequences by a sufficiently wide margin for a specific indication that the procedure is generally considered acceptable care and a reasonable approach for the indication. (Negative consequences include the risks of the procedure [i.e., radiation or contrast exposure] and the downstream impact of poor test performance such as delay in diagnosis [false negatives] or inappropriate diagnosis [false positives].)

Of the 33 CMR indications, 17 were deemed appropriate, 7 were uncertain, and 9 were rated as inappropriate (**Table 18G-1**).

The panel stressed that appropriate use criteria are not substitutes for sound clinical judgment and practice experience. Medical reasons may preclude applying the appropriate use criteria to specific patients, and clinician judgment should be used at all times in applying the criteria. For example, the rating of an indication as inappropriate should not dissuade a provider from performing CMR imaging when patient- and condition-specific data support that decision, and not performing a study rated as appropriate may be the correct decision in light of unique patient, clinical, and other relevant information.

TABLE 18G-1 Joint Professional Society* Evaluation of Appropriate Indications for Cardiac Magnetic Resonance

INDICATION	APPROPRIATENESS (MEDIAN SCORE)
Detection of CAD: Symptomatic	
Evaluation of Chest Pain Syndrome (Use of Vasodilator Perfusion CMR or Dobutamine Stress Function CMR)	
Intermediate pretest probability of CAD ECG uninterpretable or unable to exercise	A (7)
High pretest probability of CAD	U (5)
Intermediate pretest probability of CAD ECG interpretable and able to exercise	U (4)
Low pretest probability of CAD ECG interpretable and able to exercise	I (2)
Evaluation of Chest Pain Syndrome (Use of MR Coronary Angiography)	
Intermediate pretest probability of CAD ECG interpretable and able to exercise	I (2)
Intermediate pretest probability of CAD ECG uninterpretable or unable to exercise	I (2)
High pretest probability of CAD	I (1)
Evaluation of Intracardiac Structures (Use of MR Coronary Angiography)	
Evaluation of suspected coronary anomalies	A (8)
Acute Chest Pain (Use of Vasodilator Perfusion CMR or Dobutamine Stress Function CMR)	
Intermediate pretest probability of CAD No changes on the ECG and serial cardiac enzymes negative	U (6)
High pretest probability of CAD ECG—ST-segment elevation and/or positive cardiac enzymes	I (1)

Continued



TABLE 18G-1 Joint Professional Society* Evaluation of Appropriate Indications for Cardiac Magnetic Resonance—cont'd

INDICATION	APPROPRIATENESS (MEDIAN SCORE)
Risk Assessment with Prior Test Results (Use of Vasodilator Perfusion CMR or Dobutamine Stress Function CMR)	
Coronary angiography (catheterization or CT) Stenosis of unclear significance	A (7)
Equivocal stress test (exercise, stress SPECT, or stress echo) Intermediate CHD risk (Framingham)	U (6)
Normal prior stress test (exercise, nuclear, echo, MRI) High CHD risk (Framingham) Within 1 year of prior stress test	I (2)
Risk Assessment: Preoperative Evaluation for Noncardiac Surgery	
Low-Risk Surgery (Use of Vasodilator Perfusion CMR or Dobutamine Stress Function CMR)	
Intermediate perioperative risk predictor	I (2)
Intermediate- or High-Risk Surgery (Use of Vasodilator Perfusion CMR or Dobutamine Stress Function CMR)	
Intermediate perioperative risk predictor	U (6)
Detection of CAD: Postrevascularization (PCI or CABG)	
Evaluation of Chest Pain Syndrome (Use of MR Coronary Angiography)	
Evaluation of bypass grafts	I (2)
History of percutaneous revascularization with stents	I (1)
Structure and Function	
Evaluation of Ventricular and Valvular Function[†]	
Assessment of complex congenital heart disease, including anomalies of coronary circulation, great vessels, and cardiac chambers and valves Procedures may include LV-RV mass and volumes, MR angiography, quantification of valvular disease, and contrast enhancement	A (9)
Evaluation for arrhythmogenic right ventricular cardiomyopathy (ARVC) Patients presenting with syncope or ventricular arrhythmia	A (9)
Evaluation of LV function following myocardial infarction or in heart failure patients Patients with technically limited images from echocardiogram	A (8)
Quantification of LV function Discordant information that is clinically significant from prior tests	A (8)
Evaluation of specific cardiomyopathies (infiltrative [amyloid, sarcoid], HCM, or caused by cardiotoxic therapies) Use of delayed enhancement	A (8)
Characterization of native and prosthetic cardiac valves, including planimetry of stenotic disease and quantification of regurgitant disease Patients with technically limited images from echocardiogram or TEE	A (8)
Evaluation of myocarditis or myocardial infarction with normal coronary arteries Positive cardiac enzymes without obstructive atherosclerosis on angiography	A (8)
Evaluation of LV function following myocardial infarction or in heart failure patients	U (6)
Evaluation of Intra- and Extracardiac Structures	
Evaluation of cardiac mass (suspected tumor or thrombus) Use of contrast for perfusion and enhancement	A (9)
Evaluation of pericardial conditions (pericardial mass, constrictive pericarditis)	A (8)
Evaluation for aortic dissection	A (8)
Evaluation of pulmonary veins prior to radiofrequency ablation for atrial fibrillation Left atrial and pulmonary venous anatomy, including dimensions of veins for mapping purposes	A (8)
Detection of Myocardial Scar and Viability	
Evaluation of Myocardial Scar (Use of Late Gadolinium Enhancement)	
To determine viability prior to revascularization Viability assessment by SPECT or dobutamine echo has provided "equivocal" or "indeterminate" results	A (9)
To determine viability prior to revascularization To establish likelihood of recovery of function with revascularization (PCI or CABG) or medical therapy	A (9)
To determine the location and extent of myocardial necrosis, including no-reflow regions Post-acute myocardial infarction	A (7)
To detect post-PCI myocardial necrosis	U (4)

*American College of Cardiology Foundation, American College of Radiology, Society of Cardiovascular Computed Tomography, Society for Cardiovascular Magnetic Resonance, American Society of Nuclear Cardiology, North American Society for Cardiac Imaging, Society for Cardiovascular Angiography and Interventions, and Society of Interventional Radiology.

[†]Procedures may include LV and RV mass and volumes, MR angiography, quantification of valvular disease, and delayed contrast enhancement.

CABG = coronary artery bypass grafting; CAD = coronary artery disease; CHD = congenital heart disease; CMR = cardiovascular magnetic resonance; CT = computed tomography; ECG = electrocardiogram; HCM = hypertrophic cardiomyopathy; LV = left ventricular; MRI = magnetic resonance imaging; PCI = percutaneous coronary intervention; RV = right ventricular; SPECT = single-photon emission computed tomography; TEE = transesophageal echocardiography.

Since the 2006 publication of the CMR appropriate use criteria, new published data and changes in regulation and practice may influence the current appropriate use of a few specific indications. In 2008, new Current Procedural Terminology (CPT) billing codes² were created that cover assessment of blood flow and velocity quantitation by phase contrast CMR imaging. There has also been a growing body of literature indicating the strong potential usefulness for CMR in assessing acute chest pain by imaging physiologic changes at the myocardial level. This has direct relevance to the indication of "Acute Chest Pain (Use of Vasodilator Perfusion CMR or Dobutamine Stress Function CMR, Intermediate pretest probability of CAD, No changes on the ECG and serial cardiac enzymes negative," which may warrant a higher appropriate indication than its current "unknown" (U[6]). (See Table 18G-1.)

REFERENCE

1. Hendel RC, Patel MR, Kramer CM, et al: ACCF/ACR/SCCT/SCMR/ASNC/NASCI/SCAI/SIR 2006 appropriateness criteria for cardiac computed tomography and cardiac magnetic resonance imaging: A report of the American College of Cardiology Foundation Quality Strategic Directions Committee Appropriateness Criteria Working Group, American College of Radiology, Society of Cardiovascular Computed Tomography, Society for Cardiovascular Magnetic Resonance, American Society of Nuclear Cardiology, North American Society for Cardiac Imaging, Society for Cardiovascular Angiography and Interventions, and Society of Interventional Radiology. *J Am Coll Cardiol* 48:1475, 2006.
2. Centers for Medicare and Medicaid Services (<http://www.CMS.gov/Transmittals/downloads/R107ncd.pdf>).



TABLE 18-e1 Summary of the Most Common Clinical Cardiac Magnetic Resonance Pulse Sequence Techniques at the Author's Center

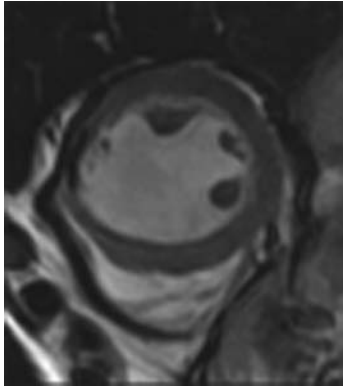
		TYPICAL IN-PLANE SPATIAL/TEMP. RESOLUTIONS AND OTHER IMAGING PARAMETERS				GADOLINIUM CONTRAST REQUIRED		RELATIVE MERITS OF THE PULSE SEQUENCE OPTIONS		IMAGE EXAMPLE
CMR TECHNIQUES	PULSE SEQUENCE OPTIONS	DARK/BRIGHT BLOOD	CONTRAST WEIGHTING	BREATH-HOLD REQUIRED	BREATH-HOLD REQUIRED	CONTRAST REQUIRED	CONTRAST REQUIRED	RELATIVE MERITS OF THE PULSE SEQUENCE OPTIONS	IMAGE EXAMPLE	
Cine cardiac structure and ventricular function	<ul style="list-style-type: none"> Cine SSFP¹ Cine FGRE Real time cine SSFP 	Bright	T2/T1W for cine SSFP and real time cine SSFP; T1W for FGRE	Yes for ECG-gated cine SSFP and FGRE; No for real time cine	No	No	<ul style="list-style-type: none"> Cine SSFP has higher SNR and CNR (between endomyocardium and blood) than FGRE but is sensitive to field inhomogeneity (especially at 3T), giving rise to banding artifact. FGRE has weaker endocardial definition than cine SSFP but is an alternative when severe artifact exists in cine SSFP Real time cine SSFP: use in patients with significant arrhythmia or difficulty breath-holding. It has the lowest spatial and temporal resolutions 	 <p>Cine SSFP</p>		
Quantitative regional myocardial strain	Myocardial tagging (newer but less widely available techniques for regional strain exist, (see text))	Bright	T1W	Yes	No	No	<ul style="list-style-type: none"> Tissue-tracking quantitation of intramyocardial motion Disadvantages: tag lines fade near end of cardiac cycle and time consuming strain analysis (post-processing) 			

TABLE 18-e1 Summary of the Most Common Clinical Cardiac Magnetic Resonance Pulse Sequence Techniques at the Author's Center—cont'd

		TYPICAL IN-PLANE SPATIAL/TEMP. RESOLUTIONS AND OTHER IMAGING PARAMETERS					GADOLINIUM CONTRAST REQUIRED		RELATIVE MERITS OF THE PULSE SEQUENCE OPTIONS		IMAGE EXAMPLE
CMR TECHNIQUES	PULSE SEQUENCE OPTIONS	DARK/BRIGHT BLOOD	CONTRAST WEIGHTING	BREATH-HOLD REQUIRED	BREATH-HOLD REQUIRED	GADOLINIUM CONTRAST REQUIRED	RELATIVE MERITS OF THE PULSE SEQUENCE OPTIONS	IMAGE EXAMPLE			
Structure, morphology, and fat imaging	<ul style="list-style-type: none"> Standard FSE† Single-shot (SS) FSE (or HASTE) 	Dark	T1W ± fat suppression	Yes for standard fast SE. No for SS FSE	No	<ul style="list-style-type: none"> Standard FSE has better image quality but relatively long scan time Fat suppression can be achieved by fat saturation pulse (more specific) or by suppressing tissues with short T1 (a technique known as STIR which is less specific for fat). SS FSE covers the whole heart quickly and is useful in patients with arrhythmia or limited breath-holding 					
Myocardial scar by LGE imaging	<ul style="list-style-type: none"> Standard 2D segmented FGRE† 2D SS SSFP technique 3D whole heart techniques (breath-hold or navigator-guided) PSIR (phase sensitive image reconstruction) 	Bright	T1W (10-30 minutes after 0.1-0.2 mmol/kg GBCA injection)	Yes for standard 2D technique. No for SS technique	Yes	<ul style="list-style-type: none"> Standard 2D technique has higher spatial and temporal resolutions than the SS technique 2D SS technique covers the whole heart quickly and is useful in patients with arrhythmia or difficulty breath-holding PSIR is inversion time insensitive and is more robust in nulling normal myocardium New 3D application using navigator-guidance yields higher SNR than 2D and can achieve spatial resolution of <1 mm without the need for breath-holding Refer to Table 18-e3 for patterns of LGE in various cardiomyopathies. 	 <p>2D segmented LGE</p>				

CMR TECHNIQUES	PULSE SEQUENCE OPTIONS	DARK/BRIGHT BLOOD	CONTRAST WEIGHTING	TYPICAL IN-PLANE SPATIAL/TEMP. RESOLUTIONS AND OTHER IMAGING PARAMETERS	BREATH-HOLD REQUIRED	GADOLINIUM CONTRAST REQUIRED	RELATIVE MERITS OF THE PULSE SEQUENCE OPTIONS	IMAGE EXAMPLE
Myocardial perfusion imaging	Saturation prepared gradient-echo based 2D techniques: - FGR ⁺ - hybrid GE-echoplanar (EPI) - SSFP	Bright	T1W	<ul style="list-style-type: none"> • 2.0-3.0 mm • 130-180 msec per slice • 3-4 locations every cardiac cycle or 6-8 locations every 2 cardiac cycles during vasodilator stress and rest. • 0.05-0.1 mmol/kg IV GBCA injected at 4 or 5 mL/sec (qualitative assessment only) 	No, but breath-hold is preferable	Yes	<ul style="list-style-type: none"> • Breath-holding useful to track contrast-enhancement in specific segments. • Parallel-imaging acceleration and sparse sampling to reduce acquisition time per slice and extend slice coverage of the heart 	

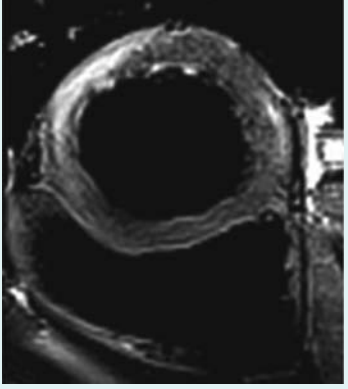
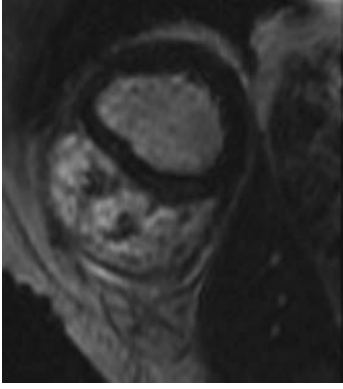

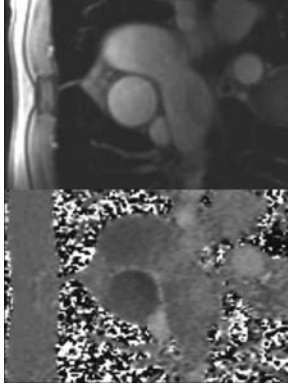
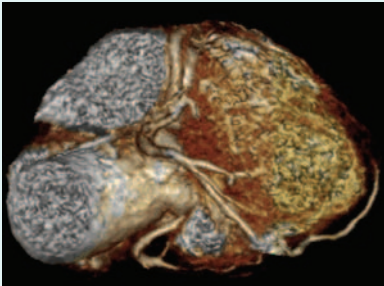
Myocardial edema imaging	<ul style="list-style-type: none"> • T2W FSE⁺ • STIR FSE • T1W EGE ratio • T2 prep SSFP • T2 map (SSFP readout) 	Dark (FSE based), Bright (SSFP based)	<ul style="list-style-type: none"> • T2W + fat suppression (for T2W techniques) • T1W (for EGE technique) 	<ul style="list-style-type: none"> • In-plane spatial and temporal resolutions similar to standard FSE • Slice thickness 7-10 mm to improve SNR • Algorithm to correct for the distance of the heart from the receiver surface coils is required 	Yes	No. Yes for EGE ratio	<ul style="list-style-type: none"> • Myocardial edema appears as a transmural area of high SI on T2W images • In FSE techniques, beware of artifacts from slow flow, especially adjacent to regional wall motion abnormality or the LV apex, which may mimic edema • Regional myocardial signal variation from phase array coils may mimic edema • In absence of LGE, T2W edema reflects reversible myocardial injury • Using T2W FSE techniques, a SI ratio of myocardium over skeletal muscle > 1.9 has been reported to be abnormal in myocarditis • An EGE ratio between myocardium and skeletal muscle of ≥ 4 or an absolute myocardial SI increase of 45% after contrast are considered abnormal in myocarditis. • The bright-blood SSFP based technique has improved CNR and is less susceptible to slow flow artifact. • T2 map is insensitive to surface coil related signal inhomogeneity and slow flowing blood related artifact 	
--------------------------	---	--	---	---	-----	-----------------------	--	--


TABLE 18-e1 Summary of the Most Common Clinical Cardiac Magnetic Resonance Pulse Sequence Techniques at the Author's Center—cont'd

		TYPICAL IN-PLANE SPATIAL/TEMP. RESOLUTIONS AND OTHER IMAGING PARAMETERS				GADOLINIUM CONTRAST REQUIRED		BREATH-HOLD REQUIRED		RELATIVE MERITS OF THE PULSE SEQUENCE OPTIONS		IMAGE EXAMPLE	
CMR TECHNIQUES	PULSE SEQUENCE OPTIONS	DARK/BRIGHT BLOOD	CONTRAST WEIGHTING	IMAGING PARAMETERS	BREATH-HOLD REQUIRED	GADOLINIUM CONTRAST REQUIRED	BREATH-HOLD REQUIRED	RELATIVE MERITS OF THE PULSE SEQUENCE OPTIONS	IMAGE EXAMPLE				
Mycardial iron content imaging	T2*W multiple echo times FGRE	Bright	T2*W	<ul style="list-style-type: none"> • 2.0–3.0 mm/ ~ 100-150 msec • One short-axis mid-ventricular location • A series of images with 8 echo times that goes from ~ 4 to 35 msec • Axial ungated acquisition of the liver for comparison 	Yes	No	<ul style="list-style-type: none"> • Measurement is most accurate and reproducible in the mid septum • T2* value describes the exponential decay of myocardial SI as the echo time increases • T2* value of < 20 msec with LV dysfunction (without other obvious cause) indicates iron-overload cardiomyopathy 						
Cardiac thrombus	<ul style="list-style-type: none"> • LGE with long inversion time • Early gadolinium enhancement (EGE) imaging 	Bright	T1W	<ul style="list-style-type: none"> • In-plane spatial and temporal resolutions similar to LGE imaging • EGE is acquired within the first 5 minutes after gadolinium injection. 	Yes	Yes	<ul style="list-style-type: none"> • LGE imaging with inversion time set at 600 msec or longer or EGE imaging can detect thrombus indicated by an intense "black" regions • Look for thrombus in locations of stagnant flows. 						
Cardiac blood flow	Phase contrast imaging cine GE	Bright	Velocity-related phase shift	<ul style="list-style-type: none"> • 1.5-2.5 mm/50 msec per phase • Keep number of lines of K space per cardiac cycle (segments) low to improve temporal resolution during free breathing studies 	No (multiple signal averages used)	No	<ul style="list-style-type: none"> • Multiple averages can reduce ghosting artifacts from respiratory motion during free breathing. • Should keep velocity encoding strength slightly > the highest expected flow velocity to avoid aliasing while maximizing accuracy 						



TYPICAL IN-PLANE SPATIAL/TEMP. RESOLUTIONS AND OTHER IMAGING PARAMETERS

CMR TECHNIQUES	PULSE SEQUENCE OPTIONS	DARK/BRIGHT BLOOD	CONTRAST WEIGHTING	BREATH-HOLD REQUIRED	GADOLINIUM CONTRAST REQUIRED	RELATIVE MERITS OF THE PULSE SEQUENCE OPTIONS	IMAGE EXAMPLE
Coronary MRA	<ul style="list-style-type: none"> 3D whole heart volume using SSFP or FGRE[†] Target-vessel approach 	Bright	T2 prepared 3D SSFP or FGRE technique	No, but Yes for target-vessel approach	Yes or No (with SSFP based technique in 1.5T)	<ul style="list-style-type: none"> Compared with the target-vessel approach, 3D coronary MRA has higher SNR and provides volumetric whole-heart coverage T2-prepared SSFP sequence with suppression of the adjacent epicardial fat provides the strong blood vessel contrast Contrast-enhanced FGRE based technique is used in 3T 	

Anatomy for electrophysiologic mapping of the pulmonary vein	<ul style="list-style-type: none"> 3D FGRE MRA of the left atrial volume and pulmonary veins 	Bright	T1W FGRE	Yes	Yes	<ul style="list-style-type: none"> Subtraction mask scan is necessary to enhance the MRA images Coronal (more common) or axial 3D MRA of the entire left atrium and the pulmonary vein is generated for electrophysiological mapping. Use same parameters as in the subtraction mask scan 	
--	---	--------	----------	-----	-----	---	--

Dark blood techniques and myocardial iron content by T2* imaging should be performed before administration of gadolinium contrast. [†] More commonly used option.

CNR = contrast to noise ratio; EGE, = early gadolinium enhancement; EPI = echoplanar imaging; FSE = fast spin echo; FGRE = fast gradient recalled echo; GBCA = gadolinium based contrast agent; GE = gradient echo imaging HASTE = Half Fourier acquisition single shot turbo spin echo; LGE = late gadolinium enhancement; MRA = magnetic resonance angiography; SE = spin echo imaging; SI = signal intensity; SNR = signal-to-noise ratio; SS = single-shot; SSFP = steady-state free precession; T1W = T1 weighted; T2*W = T2*-weighted.



TABLE 18-e2 Typical Cardiac Magnetic Resonance Protocols at Brigham and Women's Hospital

CMR STUDY INDICATIONS	CMR TECHNIQUES OF HIGH RELEVANCE	TYPICAL SCAN PLANES	OPTIONAL TECHNIQUES
Myocardial viability for benefit from coronary revascularization	<ul style="list-style-type: none"> • Cine cardiac structure/function • Low dose dobutamine cine (may depend on local expertise) • Myocardial perfusion at rest • LGE imaging for myocardial scar 	Short-axis stack and selected long-axis locations	<ul style="list-style-type: none"> • Stress myocardial perfusion • Phase contrast for co-existing valvular heart disease • Imaging for cardiac thrombus
Myocardial ischemia Vasodilating stress Dobutamine stress	<ul style="list-style-type: none"> • Cine cardiac structure/function • Myocardial perfusion at peak vasodilating stress and at rest • LGE imaging for myocardial scar • Cine function during escalating stages of dobutamine infusion ± atropine • LGE imaging for myocardial scar 	Short-axis stack and selected long-axis locations 3 short-axis and 2 or 3 long-axis locations for stress cine	<ul style="list-style-type: none"> • Myocardial perfusion during dobutamine stress
Acute myocardial infarction	<ul style="list-style-type: none"> • Cine cardiac structure/function • Myocardial edema imaging • Myocardial perfusion at rest • LGE imaging for myocardial scar 	Short-axis stack and selected long-axis locations	<ul style="list-style-type: none"> • Imaging for cardiac thrombus and microvascular obstruction (no-reflow)
Detecting ACS or other causes of myocardial injury	<ul style="list-style-type: none"> • Cine cardiac structure/function • Myocardial edema imaging • Myocardial perfusion at rest • LGE imaging for myocardial scar 	Short-axis stack and selected long-axis locations	<ul style="list-style-type: none"> • Stress myocardial perfusion
Assessing the etiology of an undiagnosed cardiomyopathy or a specific cardiomyopathy	<ul style="list-style-type: none"> • Cine cardiac structure/function • Myocardial perfusion at rest • Myocardial edema imaging (if acute myocarditis, ACS, or infiltrative CMP suspected) • LGE imaging for myocardial scar 	Short-axis stack and selected long-axis or axial locations	<ul style="list-style-type: none"> • Myocardial and hepatic iron content (if cardiac hemochromatosis suspected) • Stress myocardial perfusion (if CAD suspected) • FSE with and without fat suppression (if ARVC suspected) • Phase contrast flow imaging (if outflow obstruction suspected in HCM) • Myocardial T1 quantitation (amyloidosis)
Pericardial disease	<ul style="list-style-type: none"> • Cine cardiac structure/function • T1W FSE without fat suppression to assess pericardium (low-intensity linear structure that lies between high-intensity mediastinal and epicardial fat) • Myocardial edema imaging (if acute myocarditis, ACS, or infiltrative CMP suspected) • LGE imaging for myocardial scar 	Short-axis stack and selected long-axis or axial/oblique locations	<ul style="list-style-type: none"> • Myocardial tagging to assess perimyocardial adhesions in region of reduced strain • Imaging for sizes of the vena cava • Real-time cine SSFP (to see septal motion) and phase contrast flow across the tricuspid valve for pericardial constriction. • T1W and T2W techniques to assess fluid content of significant pericardial effusion. Transudative effusion is gray or dark on T1W and bright on T2W images. Exudative effusion is bright and subacute hemorrhage is inhomogeneous on T1W images
Valvular heart disease	<ul style="list-style-type: none"> • Cine cardiac structure/function • Phase contrast flows of the dysfunctional valve of interests →Use appropriate velocity-encoding strengths to obtain peak velocity (valvular stenosis) and forward/regurgitant flows (valvular insufficiency) • Imaging of the great vessels (Fast SE, MRA, or others) 	Short-axis stack and selected long-axis or axial/oblique locations	<ul style="list-style-type: none"> • LGE for myocardial scar (e.g., severe aortic stenosis)
Cardiac mass/Thrombus	<ul style="list-style-type: none"> • Cine cardiac structure and function (size, attachment, and motion pattern of the mass). • T1W imaging before and after contrast to assess vascularity of the mass • FSE to assess fat content and structure. • T2W FSE to look for tissue edema or simple cyst 	Short-axis stack and selected long-axis or axial/oblique locations	<ul style="list-style-type: none"> • EGE or LGE with long inversion time to assess for thrombus • First-pass perfusion to assess mass with high vascularity • LGE to detect necrosis.
CMR for left atrial mapping and pulmonary vein ablation	<ul style="list-style-type: none"> • Cine cardiac structure/function • 3D FGRE MRA imaging of the left atrial volume and pulmonary veins 	Short-axis stack and selected long-axis Coronal 3D locations for MRA	<ul style="list-style-type: none"> • Phase contrast imaging prescribed as cross sections of the origins of the pulmonary veins from the coronal MRA images. Use encoding velocity strength of 30 cm/sec for normal flow and increase if pulmonary stenosis suspected or aliasing detected • High-resolution LGE imaging of the left atrial scar (with navigator guidance) has been reported by experienced centers in patients who had undergone radiofrequency ablation of the left atrium

ACS = acute coronary syndrome; ARVC = arrhythmogenic right ventricular cardiomyopathy; CAD = coronary artery disease; CMP = cardiomyopathy; CMR = cardiac magnetic resonance imaging; HCM = hypertrophic obstructive cardiomyopathy; T2W = T2 weighted.

TABLE 18-e3 Findings from Cardiac Magnetic Resonance That Differentiate the Etiologies of Cardiomyopathy

CMR STUDY INDICATIONS	CINE CARDIAC STRUCTURE/FUNCTION	MYOCARDIAL EDEMA	MYOCARDIAL PERFUSION	LGE IMAGING	ASSOCIATED CMR FINDINGS
Acute myocardial stunning	RWMA	Positive	Normal (at rest)	Normal	<ul style="list-style-type: none"> Stress perfusion may show perfusion defect during peak vasodilatation (if significant residual coronary stenosis exists) Coronary MRA may show luminal stenosis
Chronic myocardial hibernation	RWMA, regional wall thinning possible	Negative	Usually shows resting subendocardial perfusion defect in a coronary distribution	Normal	<ul style="list-style-type: none"> Stress perfusion shows larger extent of perfusion defect than at rest (reversible defect) in regions without LGE Intracavitary thrombus may exist in areas of stagnant flow
Acute MI	RWMA	Usually transmural bright region in the segments subtended by the infarct-related artery	Subendocardial perfusion at rest (given revascularization of infarct-related artery) represents no-reflow zone of infarction	Subendocardial or transmural LGE in a coronary distribution	<ul style="list-style-type: none"> Microvascular obstruction "no-reflow" may be seen by LGE or myocardial perfusion imaging Evidence of myocardial hemorrhage by T2 and T2* imaging has been described Intracavitary thrombus may exist in areas of stagnant flow
Chronic MI	RWMA, chronic remodeling changes	Negative	Subendocardial defect at rest matching thinned infarcted region, but can be normal in small infarcts after coronary revascularization	Thinned subendocardial or transmural LGE in a coronary distribution	<ul style="list-style-type: none"> Intracavitary thrombus may exist in areas of stagnant flow
Myocardial ischemia	Normal or RWMA	Negative	Reversible subendocardial perfusion defect in a coronary distribution	Normal	<ul style="list-style-type: none"> Subendocardial perfusion defect from significant coronary stenosis should persist beyond peak myocardial enhancement during first-pass transit of GBCA bolus Coronary MRA may show luminal stenosis
Idiopathic dilated CMP	Dilated hypocontractile LV/RV	Negative	Normal	Mid-wall LGE often in the septum	<ul style="list-style-type: none"> Mitral regurgitation secondary to dilated ventricle and mitral annulus may be present
HCM	Increased ventricular mass. Asymmetric septal hypertrophy in some cases with or without LV outflow obstruction. Spade-shaped LV chamber in apical HCM.	Often abnormal	Abnormal in thickened myocardial segments may represent abnormal microcirculation	LGE at RV insertion into LV or patchy mid-wall involvement in the hypertrophied segments	<ul style="list-style-type: none"> Outflow or mid ventricular obstruction by phase contrast imaging Systolic anterior motion of mitral leaflet \pm mitral regurgitation May show reduced intramyocardial motion in hypertrophic regions Reversible perfusion defect may indicate abnormality of the coronary microcirculation.
ARVC	RV dilated/aneurysmal	Negative	Normal	RV often full thickness LGE matching location of the RV aneurysm \pm LV focal LGE	<ul style="list-style-type: none"> Fatty infiltration of RV and LV focally may be seen by T1W FSE imaging and confirmed by fat suppression techniques "Nulling" of normal myocardium of the RV and the LV needs different inversion (TI) times.

TABLE 18-e3 Findings from Cardiac Magnetic Resonance That Differentiate the Etiologies of Cardiomyopathy—cont'd

CMR STUDY INDICATIONS	CINE CARDIAC STRUCTURE/FUNCTION	MYOCARDIAL EDEMA	MYOCARDIAL PERFUSION	LGE IMAGING	ASSOCIATED CMR FINDINGS
Acute myocarditis	RWMA and/or hypocontractile LV	Usually transmural bright regions are seen, can be patchy or diffuse	Normal	Epicardial and mid-wall LGE involving inferolateral wall or septum	<ul style="list-style-type: none"> Pericardial involvement or effusion possible
Cardiac sarcoidosis	RWMA and/or hypocontractile LV/RV	Bright regions representing myocardial edema are variable	Normal	Multi-focal intense LGE often involving the septum, inferolateral wall of the LV, right atrium, and RV free wall	<ul style="list-style-type: none"> Mediastinal lymphadenopathy
Cardiac amyloidosis	Restrictive morphology, reduction of systolic thickening in LGE segments	Negative	Diffuse perfusion defect common	Diffuse circumferential (often subendocardial) LGE	<ul style="list-style-type: none"> Rapid gadolinium wash-out from LV blood pool after injection Difficulty in finding the right inversion time in “nulling” normal myocardium during LGE imaging Low endocardium/blood T1 ratio several minutes after contrast injection Thickened atrial walls with atrial LGE, loss of atrial contraction
Iron-overload CMP	Hypocontractile LV with dark myocardium	Negative	Normal	Normal	<ul style="list-style-type: none"> Very low hepatic T2* value
LV non-compaction	Hypocontractile LV with sponge-like trabeculae often in the lateral wall and the apex.	Negative	Normal	Mid-wall or focal LGE	<ul style="list-style-type: none"> May see intracavitary thrombi
Apical ballooning syndrome	Circumferential ballooning and RWMA of all apical segments	Bright regions primarily involve the apical segments	Normal	Normal or only minimal subendocardial LGE	<ul style="list-style-type: none"> Patchy intermediate-intensity LGE without loss of wall thickness and T2W evidence of myocardial edema can be seen Reversal of abnormal findings after stressful events helps diagnosis.
Endomyocardial disease	Dilated hypocontractile LV and/or RV	Negative	Normal	Diffuse subendocardial LGE of LV or RV ± thrombus	<ul style="list-style-type: none"> Cavitary thrombus can be seen on cine SSFP or LGE imaging with long inversion time. May be extensive to obliterate the LV or the RV apex
Fabry disease	Concentrically thickened LV ± RWMA with wall thinning	Negative	Normal	Mid-wall LGE often in the inferolateral wall	<ul style="list-style-type: none"> Associated evidence of CAD possible
Chagas disease	Often presents as dilated and severe hypocontractile LV during the latent period of the disease	Negative in the latent period, positive if presented acutely	Normal	Resemble the pattern of healed viral myocarditis with epicardial LGE involving the inferolateral wall common. Apical aneurismal changes have been described.	—
Acute pericarditis	Often normal; pericardial effusion	Positive if myocardial involvement	Normal	Often normal but may see diffuse pericardial enhancement	<ul style="list-style-type: none"> Pericardial thickness often normal CMR is better than echocardiography in assessing the extent and loculation of pericardial effusion

TABLE 18-e3 Findings from Cardiac Magnetic Resonance That Differentiate the Etiologies of Cardiomyopathy—cont'd

CMR STUDY INDICATIONS	CINE CARDIAC STRUCTURE/FUNCTION	MYOCARDIAL EDEMA	MYOCARDIAL PERFUSION	LGE IMAGING	ASSOCIATED CMR FINDINGS
Chronic pericardial constriction	Small heart, large atria, and abnormal septal motion with respiratory variation during real-time cine imaging.	Negative	Normal	Diffuse pericardial enhancement. Myocardial involvement possible	<ul style="list-style-type: none"> • Diffuse thickening (>3mm) of pericardium seen by T1W FSE • Constrictive tricuspid inflow pattern by phase contrast • Bilateral pleural effusions. • Enlarged vena cavae and tubular-shaped RV
Cardiac mass	Proximity to a RWMA or a catheter, atrial fibrillation, recent endovascular procedure are associated with thrombus	Thrombus is dark on T2W imaging High SI may indicate edema with tumor mass	Thrombus is dark on first-pass perfusion imaging Cardiac tumors have variable degree of enhancement on first-pass perfusion	Mural thrombus may have an "etched" appearance on LGE imaging May see LGE within tumor mass from fibrosis	<ul style="list-style-type: none"> • Most malignancy is metastatic rather than primary. • Recognize common normal structures: Eustachian valve, Chiari network, crista sagittalis or terminalis, RV moderator band, and interatrial septal aneurysm • Beware of "pseudotumors:" coronary or aortic aneurysm, lipomatous hypertrophy of the interatrial septum, hiatal hernia, or catheters etc.

ARVC = arrhythmogenic right ventricular cardiomyopathy; LV = left ventricular; MI = myocardial infarction; RWMA = regional wall motion abnormalities; RV = right ventricular.